Deep-Sea Research II 56 (2009) 2409–2426

Contents lists available at ScienceDirect

Deep-Sea Research II

journal homepage: www.elsevier.com/locate/dsr2

Modeled transport of freshwater from a line-source in the coastal Gulf of Alaska

Elizabeth L. Dobbins [a], Albert J. Hermann [a,*], Phyllis Stabeno [b], Nicholas A. Bond [a], Richard C. Steed [c]

[a] Joint Institute for the Study of the Atmosphere and Ocean, University of Washington, P.O. Box 357941, Seattle, WA 98195, USA
[b] NOAA/Pacific Marine Environmental Laboratory, 7600 Sand Point Way NE, Seattle, WA 98115, USA
[c] Department of Atmospheric Science, University of Washington, P.O. Box 351640, Seattle, WA 98195, USA

ARTICLE INFO

Article history:
Accepted 26 February 2009
Available online 19 March 2009

Keywords:
Coastal oceanography
Coastal currents
Mathematical models
Ocean circulation
Physical oceanography
Alaska Coastal Current

ABSTRACT

A set of multiply nested atmospheric (The Penn State/NCAR Mesoscale Modeling system—MM5) and oceanic (Regional Ocean Modeling System—ROMS) models has been developed to investigate ecosystem forcing as part of the US. GLOBEC program. This study focuses on the most finely nested oceanic model in the hierarchy, that of the coastal Gulf of Alaska (CGOA) during 2001–2002, and compares the model's results to data collected by GLOBEC investigators. The 3-km resolution model realistically generates two physical features needed to reproduce the CGOA ecosystem: the cross-shelf water mass structure on the Seward Shelf, and the seasonal cycle of vertical structure. In addition, the temporal variability of currents and tracer fields generated by the model is greatly improved compared to previous work, as is the resolution of the Alaska Coastal Current (ACC). However, the treatment of the line-source freshwater source along the coast of Alaska still presents difficulties, because the model cannot resolve the many inlets and fjords where mixing takes place initially. This issue is investigated by testing the model's sensitivity to various forcing mechanisms which could compensate for this weakness, such as the addition of tidal mixing, the use of finely resolved winds, and the use of brackish runoff rather than purely freshwater for the line-source.

1. Introduction

In the coastal Gulf of Alaska (CGOA), high phytoplankton production supports several commercially important fisheries (OCSEAP Staff, 1987; Sambrotto and Lorenzen, 1987). However, because the CGOA shelf is forced by downwelling favorable winds for most of the year (Royer, 1998), the source of the nutrients that drive this productivity is not obvious. Recent field and modeling work funded by the Global Ocean Ecosystem Dynamics (GLOBEC) Northeast Pacific (NEP) Program , and focused on the shelf near Seward, Alaska, has made progress in answering this critical question (Weingartner et al., 2002). The regional circulation model described here will be used in papers to investigate dynamics and mechanisms (Hermann et al., 2009b).

One of the early GLOBEC hypotheses about the ecosystem in the CGOA is that the spatial and temporal variability of the mesoscale circulation field constitutes the dominant physical forcing on zooplankton biomass (US GLOBEC, 1996). The GLOBEC program attempts to examine the consequences of future climate change by first characterizing the variability of the present system. Coupled biophysical models form a critical centerpiece intended to integrate field measurements across space, time, and scientific discipline so that the overall picture can be extrapolated into the future. However, this process requires that the physical model accurately reproduces the interannual and mesoscale circulation features, and that the biological model accurately translates these to ecosystem effects. This paper attempts to validate the aspects of the physical model that are most critical to addressing GLOBEC hypotheses, and the companion paper (Hinckley et al., 2009) does the same for the biological component.

Circulation near the Seward shelf is dominated by the Alaskan Stream (AS) off-shore and the Alaska Coastal Current (ACC) on-shore (Fig. 1). The area can be divided into several cross-shelf regimes that have distinct biological and chemical qualities. The Copper River and distributed runoff along the coast supplies iron-rich, but otherwise nutrient-poor water to the shelf (Feely et al., 1981); the basin, on the other hand, is a high-nutrient low-chlorophyll (HNLC) region believed to be iron limited (Martin et al., 1989; Boyd et al., 1996). Recent hypotheses on the driving mechanisms of the high shelf productivity hinge on the importance of cross-shelf transport, and the interactions between the two current systems within a meandering, highly variable, transition zone (Weingartner et al., 2002; Stabeno et al., 2004;

* Corresponding author.
E-mail address: Albert.J.Hermann@noaa.gov (A.J. Hermann).

0967-0645/$ - see front matter © 2009 Elsevier Ltd. All rights reserved.
doi:10.1016/j.dsr2.2009.02.004

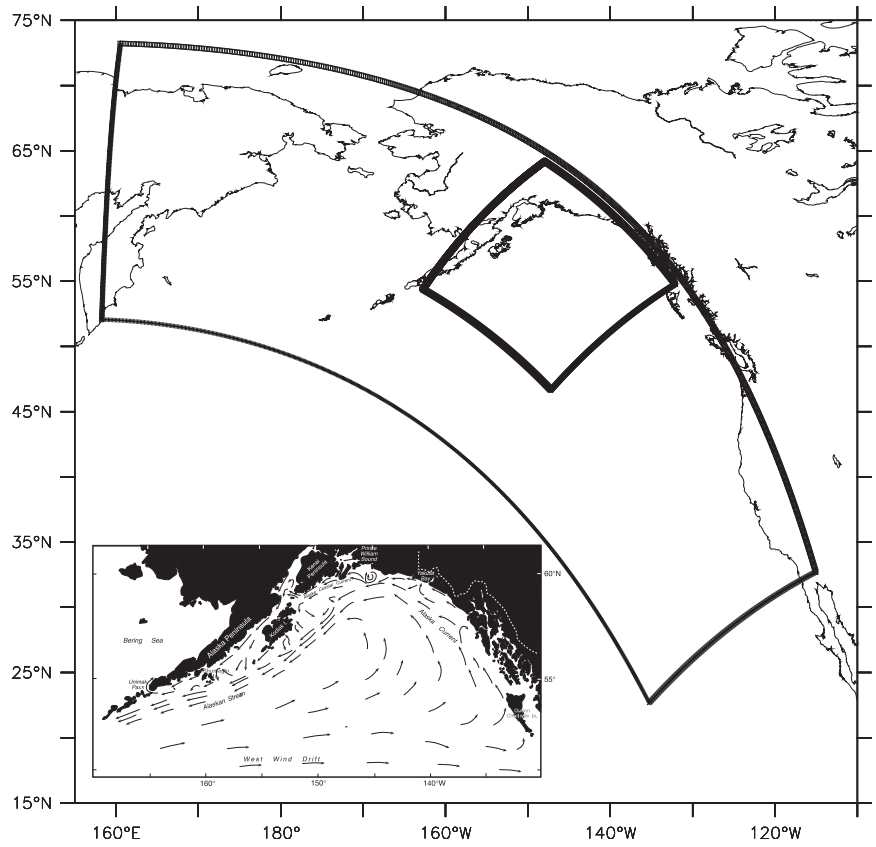

Fig. 1. Boundaries of the NEP model (large box) and CGOA model (small box). Inset of the coastal Gulf of Alaska with its major current systems.

Ladd et al., 2005b). It is therefore critical that the circulation model reproduce the physics of this cross-shelf structure.

Successful modeling of the annual biological cycle depends on replicating the vertical structure seen in the field. Vertical mixing in the winter and spring primes the water column for the spring bloom by mixing nutrient-rich water upwards (Childers et al., 2005). As wind mixing decreases, the spring bloom develops first in the stratified water of the ACC (Napp et al., 1996). As stratification develops in the summer, so does a nutrient-depleted surface layer and subsurface chlorophyll maximum (Sambrotto and Lorenzen, 1987; Childers et al., 2005). The circulation model is used to replicate this annual cycle of stratification and mixing. It also will be used in Hermann et al. (2009b) to quantify the nutrient addition to the surface layer that is due to horizontal wind shear via upwelling; this analysis will depend on replication of the correct vertical structure.

To replicate these two important features—vertical and cross-shelf structure—the model must deal with forcing at a wide range of spatial scales, from basin-scale events such as El Niño to the narrow ACC. At local scales, the cross-shelf extent of the ACC varies in response to seasonal cycles in downwelling winds and runoff (Royer, 1981); the internal Rossby radius varies spatially and seasonally between 5 and 20 km, with minimum values in the winter (Royer, 1998; Weingartner et al., 2005). Runoff, summarized by the freshwater inflow rate Q, is high in the CGOA with total discharge estimated at 24,000 $m^3 s^{-1}$ (40% of the total freshwater input into the Pacific), and it is distributed in countless streams and small rivers (Royer, 1982) rather than in a single river mouth. The distribution of this freshwater inflow impacts cross-shelf transport. Models of the South Atlantic Bight suggest that during periods of downwelling winds, cross-shelf transport is more restricted when freshwater is input as a line-source than when it is a point source, and that during periods of upwelling winds, the off-shore transport of a line-source is most pronounced at its upstream end, or head (Kourafalou et al., 1996).

Accurate surface forcing at regional scales represents another challenge to successfully model the CGOA. Passing storms are trapped by the mountainous terrain that surrounds the CGOA, intensifying winds and producing large amounts of precipitation in coastal watersheds (Stabeno et al., 2004). Large-scale gridded atmospheric data sets do not resolve the orographic steering caused by these mountains; comparison with the NCEP/NCAR reanalysis product (NCEP) (Kalnay et al., 1996; Kistler et al., 2001) found that measured wind speeds are about 50% higher than NCEP winds during periods of southerly or easterly along-shore winds (Stabeno et al., 2004). Idealized 3-D modeling results (Williams et al., 2007) show that higher magnitude downwelling wind, τ, results in reduced buoyancy accumulation on this section of the shelf as the coastal current width, Y, narrows according to:

$$Y \approx L_D \left(\frac{Qf}{\tau/\rho 0} \right)^{1/2}$$

where

$$L_D = \frac{\sqrt{g' H_{\max}}}{|f|} \quad \text{and} \quad H_{\max} = \left(\frac{2Qf}{g'} \right)^{1/2} x^{1/2}$$

where Q is the freshwater inflow rate, f is the Coriolis frequency, ρ_0 is the background density, L_D is the Rossby radius of deformation, g' is the reduced gravity of the buoyant inflow, H_{max} is the coastal current depth limit, and x is along-shelf distance. Accurate estimation of surface wind forcing is therefore critical, since it is mainly salinity which controls the horizontal and

vertical density gradients on the shelf (Royer, 1998; Stabeno et al., 2004).

At mid-shelf locations, modeling the Seward Shelf is complicated by a wide variety of instabilities that cause variations in ACC transport. Modeling of the Shelikof Strait region determined that whereas the ACC's barotropic transport depends strongly on wind forcing, high buoyancy forcing results in the generation of eddies and increased cross-shelf flow (Hermann and Stabeno, 1996; Stabeno and Hermann, 1996). Similar features arising in an idealized model of Alaska's coastal current were apparently baroclinic instabilities associated with increased along-shelf flow speed and cross-shelf shear; instabilities increased the width of the coastal current so that buoyancy accumulated on the shelf (Williams et al., 2007). The bathymetry near Seward is particularly complex, so the on-shore transport of nutrients also can be affected by local, small-scale canyons and banks via direct topographic steering, inertial overshoot of along-shore flow, and modification of upwelling and downwelling (Stabeno et al., 2004; Ladd et al., 2005b). Complex bathymetry is expected to shed additional shelf eddies and meanders in the ACC (Childers et al., 2005; Weingartner et al., 2005). The budget of freshwater on the shelf in Alaska, and its fate downstream, is an active area of research, but previous studies have been limited by their inability to estimate the loss of freshwater to the oceanic basin through instabilities and exchange over the shelf-break (Williams et al., 2007; Weingartner et al., 2005); a fully 3-D model could be used to address this limitation. Finally, large (200 km) "basin" eddies are advected into the region from their generation locations upstream and affect the shelf-break region (Okkonen et al., 2003; Stabeno et al., 2004; Childers et al., 2005; Ladd et al., 2005a, 2009).

Tides also modify the structure of ACC in ways that should be included in our modeling effort. Though there is significant spatial variability along the coast (Stabeno et al., 2004), at some locations along the northern CGOA shelf, tides are responsible for 80% of the energy measured by current meters (Ladd et al., 2005b). In fact, Cook Inlet and the banks around Kodiak Island account for 76% of M2 tidal dissipation in the Northeast Pacific (Foreman et al., 2000). Tidal information applied to the boundaries of an earlier circulation model of the CGOA modified SST and subtidal currents only in these shallow areas (Hermann et al., 2002). In other models, such interactions are strong in coastal regions; addition of tidal mixing in a 3-D primitive model of the South Atlantic Bight increased cross-shelf gradients of density and surface elevation, enhancing the along-shelf current and slowing the off-shore transport of water (Chen, 2000).

2. Methods

2.1. Ocean model

2.1.1. Configuration

Using the Regional Ocean Modeling System (ROMS) (Haidvogel et al., 2000; Shchepetkin and McWilliams, 2003), we construct an embedded set of three grids of increasing resolution, each of which supplies initial and boundary conditions for the next finer grid (Fig. 1). The grid domains include the North Pacific (NPac, 40 km, Curchitser et al., 2005), the Northeast Pacific (12 km, Hermann et al., 2009a), and the coastal Gulf of Alaska (3 km), which is the focus of this paper. The southwest and southeast boundaries of the CGOA domain are open, which allows entry (exit) of the Alaskan Stream from (into) the NEP domain. The focus of the CGOA domain, and this study, is the shelf off-shore of Seward, Alaska (the Seward Shelf, also known as the Kenai Shelf), where GLOBEC's LTOP program collected the data used to validate the model. The domain extends along the southeast Alaskan coast to include the generation locales of basin-scale eddies and the entire input region of Alaska's freshwater line-source. These features exert an important influence on the GLOBEC study area, but are not expected to be fully resolved by the NEP grid.

The CGOA grid is Cartesian, has 482×482 horizontal points, and has 30 vertical levels that are concentrated near the surface (ROMS stretching parameters $q_S = 5$ and $q_B = 0.4$). The grid's surface layer is ~0.3 m in the shallowest areas (10 m deep), ~7.5 m at the shelf-break, and ~15 m over the basin (6000 m deep). ETOPO5 bathymetry (NGDC, 1988), improved in the coastal areas of the Gulf of Alaska through the addition of supplemental data (Hermann et al., 2002), was smoothed using a selective Shapiro filter. Between passes of the smoothing filter, the depth at the coastline was raised so that shallow areas on the shelf would be retained after the filtering. For our 3-km grid, this procedure retains the complex pattern of canyons and banks that intersect the shelf, and provides resolution of at least four grid-points on the shelf (Fig. 2); the resulting maximum slope parameter, $r = \Delta h/2h$, where h is the bottom depth, has a value of 0.342 (Beckmann and Haidvogel, 1993).

ROMS, version 2.0, is a hydrostatic, primitive equation, generalized sigma-coordinate model. The time stepping scheme is described in Haidvogel et al. (2000); the baroclinic time step was 240 s, with 30 barotropic time steps per baroclinic time step. The pressure gradient discretization is the density Jacobian scheme (Shchepetkin and McWilliams, 2003). The third-order upstream bias scheme for horizontal advection (Shchepetkin and McWilliams, 1998) is used for tracers and 3-D momentum. This scheme results in implicit weak smoothing at the smallest grid scales, which reduces the need for explicit horizontal diffusion and viscosity. Vertical advection of tracers is handled with a parabolic splines scheme, allowing longer time steps. Vertical tracer and momentum mixing is achieved via the K-profile parameterization (KPP) for interior mixing (Large et al., 1994); the KPP options used with ROMS here include convective nonlocal transport, diffusivity due to shear instability, and surface and bottom boundary layers. The KPP scheme responds to changes in stratification generated at the surface by heating due to shortwave radiation's penetration of the water column, and surface freshwater flux. The bottom boundary layer extension to KPP, similar in form to the surface boundary layer, combines interior and boundary layer mixing rates when the surface and bottom boundary layers interact in nearshore areas (Durski et al., 2004). Quadratic bottom drag, with a coefficient of 0.003 (non-dimensional), is used. A no-slip boundary condition is applied at masked land areas. The Coriolis force varies with latitude.

2.1.2. Boundaries/model coupling

The set of nested grids employs one-way nesting at the grid boundaries; daily physical fields generated by the 12-km resolution NEP grid are interpolated to the locations of the 3-km CGOA grid's southwest and southeast boundary points. Because the CGOA grid is a subregion of the NEP grid, with the same orientation relative to north, velocities are not rotated. No attempt is made to match the interpolated transport to that produced by the NEP model. Tracer and 3-D momentum fields at CGOA's open boundaries are relaxed to these values using a radiative boundary condition with adaptive nudging as described by Marchesiello et al. (2001). The radiation condition determines if information is propagating inward or outward at each boundary point, and uses an appropriate nudging time scale in each case. Nudging time scales are three days for active/inflow boundary conditions, and one year for passive/outflow boundaries. The gentle nudging at outflow locations allows disturbances to propagate out of the

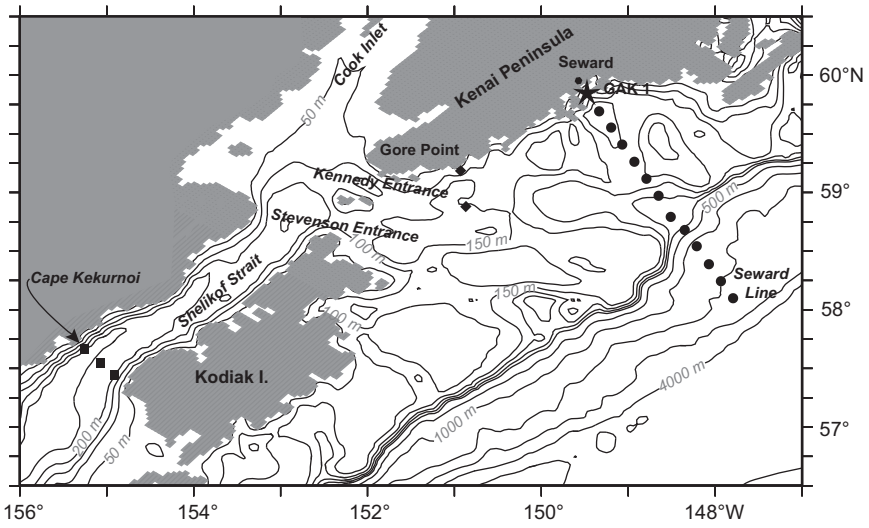

Fig. 2. CGOA model bathymetry. GAK-1 mooring location is indicated by a star, Cape Kekurnoi ADCP current meter moorings by squares, and Gore Point moorings by diamonds. Hydrographic stations along the Seward line are marked with dots. GAK-1 is labeled; other stations are numbered 2–13, with 13 farthest off-shore.

CGOA model while insuring that the interior model solution does not drift away from the boundary conditions. The Chapman scheme is used for the free surface (Chapman, 1985).

Because tidal information is not available from the 12-km NEP grid, tidal forcing of the CGOA is accomplished by supplementing the Flather boundary conditions (Flather, 1976) derived from the NEP model with barotropic velocity and sea-surface height generated by a high-resolution, data assimilating, finite element, barotropic model of the Northeast Pacific Ocean (Foreman et al., 2000). Four diurnal (O1, Q1, P1, and K1) and four semidiurnal (N2, S2, K2, and M2) tidal constituents are used, with amplitudes from the barotropic model. These are applied at the open boundaries of the CGOA grid, and tidal signals are allowed to propagate freely throughout the CGOA domain. The results do not exactly replicate tidal currents at a particular place or time, as the tidal components are applied without phasing for a specific calendar date. However, it does generate a reasonable approximation of tidal effects such as mixing, which appear, even in this rough form, to be essential to reproducing some elements of CGOA circulation, as will be shown in Section 3.3.2.

High tidal velocities, especially in Kennedy and Stevenson Entrances near the mouth of Cook Inlet, require relatively high horizontal viscosity (or a very small time step) to keep the model stable; we employ harmonic (Laplacian) mixing along constant S-surfaces with a viscosity coefficient of $100\,m^2\,s^{-1}$. This amount of viscosity still allows the formation of eddies and meanders. Increased mixing is also required near the open boundaries to dampen spurious boundary signals; within 10 points of the open boundaries, viscosity is ramped up to $250\,m^2\,s^{-1}$. Tracers are mixed along geopotential surfaces, and in the same 10 points of the open boundaries, the diffusivity coefficient is ramped from zero in the interior to $200\,m^2\,s^{-1}$ at the boundaries.

2.1.3. Forcing

Surface heat and momentum flux is calculated internally from daily average atmospheric variables and the TOGA-COARE bulk algorithms (Fairall et al., 1996); input variables include winds, sea level pressure, humidity, clouds, rain, longwave radiation, and relative humidity. Two different sources of atmospheric forcing are used. The first is coarse-scale fields from NCEP/NCAR Global Reanalysis Project (NCEP; Kalnay et al., 1996), which have a native resolution of 2.5° latitude and longitude. The second source is much finer-scale fields from a relatively high-resolution simulation by the Penn State/NCAR Mesoscale Model (MM5; Dudhia, 1993). Configuration of the MM5 model is discussed in Section 2.2, and sensitivity of the CGOA model to these two sets of inputs is discussed in Section 3.3.1. The primary objective for using the MM5 was to better account for orographic effects on the mesoscale forcing in the coastal zone.

Shortwave radiation is calculated analytically, varies with location, day of year, and time of day (Zillman, 1972), and is corrected for cloud fraction (Laevastu, 1960) as described by Parkinson and Washington (1979). Vapor pressure for the cloud correction is derived from relative humidity and surface air temperature (Gill, 1982). Both NCEP and MM5 overestimate shortwave radiation (by $\sim 70\,W\,m^{-2}$) in the Bering Sea because they underestimate low-level stratus clouds (Ladd and Bond, 2002). To allow decades-long runs of the NPac (basin-scale) model without the distorting effects of surface nudging, the solar constant was reduced to $700\,W\,m^{-2}$; for consistency, this value was carried through to the NEP and CGOA grids as well. Comparison of the model-generated shortwave radiation with values measured by a mid-shelf surface mooring (station GAK-3; 59.27N, 149.0W) show that daily means are underestimated by approximately $70\,W\,m^{-2}$ in the summer and by $10\,W\,m^{-2}$ in the fall and winter (Fig. 3B); R^2 values for model-data correlation during these periods are 0.38 and 0.74 (both significant at the 1% level).

The monthly freshwater input from land to the CGOA is derived from snowpack, precipitation, and temperature data, integrated along the entire Alaskan coast (T. Royer, pers. comm.). These data (Fig. 3C) are applied equally to 1176 grid-points along the edge of the model's land mask between Ketchikan (at the model's southeast boundary) and the Kenai Peninsula; the freshwater volume is applied to the topmost vertical cell at each of these grid-points. The line-source's salinity and temperature are set to monthly climatological values calculated from LTOP measurements at the surface of the innermost Seward Line station (GAK-1). The resulting brackish water produced by tracers which vary seasonally is meant to simulate mixing in fjords/estuaries which are not resolved in this model. A similar approach was taken by Williams et al. (2007), although we do not alter the input volume as presented in that study, because the amount of extra

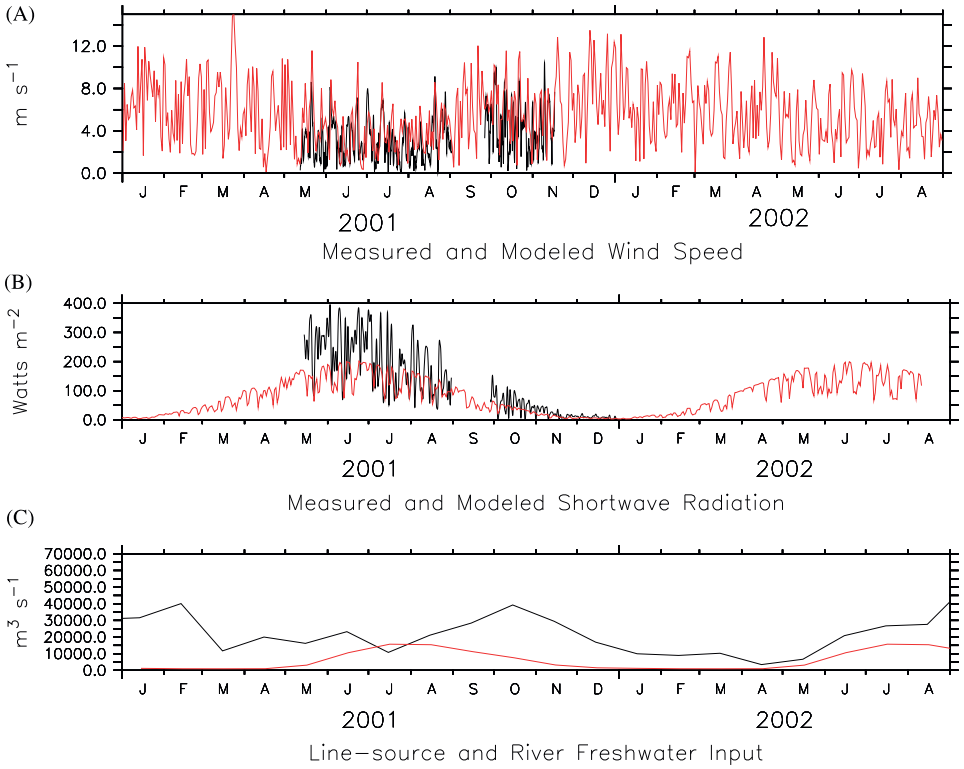

Fig. 3. Forcing used by the model compared with measured values: (A) measured (black) and MM5 modeled (red) wind speed ($m\,s^{-1}$), (B) averaged daily measured (black) and modeled (red) shortwave radiation ($W\,m^{-2}$) and (C) freshwater runoff ($m^3\,s^{-1}$) from distributed line-source (black) and sum of larger rivers (red).

Table 1
Summary of physical forcing variations for all model runs.

Case	Surface forcing	Tides	Line-source salinity	Line-source vertical profile	Years
A	MM5	Yes	Brackish	Surface	2001–2002
B	NCEP	Yes	Brackish	Surface	2001
C	MM5	None	Brackish	Surface	2001
D	MM5	Yes	Fresh	Surface	2001 (partial)
E	MM5	Yes	Fresh	Vertical ramp	2001

water required to create a line-source with the correct salinity unrealistically increases ACC transport (not shown). Sensitivity tests (Section 3.3) reveal that the vertical profile and salinity of this input are critical for generating the correct vertical stratification on the shelf. River discharge for five gauged rivers—the Copper, Alsek, Stikine, Taku, and Susitna—are also included since they drain the land's interior and are not expected to be included in the line-source estimation. The rivers were not gauged every year, so repeating monthly climatologies of volume were produced for use with the model (K. Carney, pers. comm.); using climatologies should not affect interannual signals substantially since the volume of freshwater contributed by the rivers is much lower than the line-source's volume. Rivers and the line-source were treated somewhat differently in the NEP grid, but NEP still presents a fully spun-up (albeit coarsely resolved) ACC in the initialization for the CGOA grid (Hermann et al., 2009a). The largest grid, NPAC (Curchitser et al., 2005), has no rivers or line-source.

2.1.4. Model execution and performance

The CGOA model was initialized in December 2000, with results from the NEP grid run with NCEP forcing from 1996 to 2000. All model variables were filtered during the running of the model with a 40 h Cosine–Lanczos filter to remove tidal aliasing before the daily values were output. Variations of the model were run to assess the model's success in accounting for the CGOA's unique environment as it is described in Section 1. Specifically, we tested the effects of fine scale winds (which required development of the high-resolution atmospheric model), tidal forcing (which adversely affected the model's stability), and the form of the line-source runoff (whose configuration is a work in progress) with the following runs (Table 1):

Case A: This "Base Case" was run with tidal and MM5 forcing for 2001 and 2002. Lateral boundary conditions were supplied by the NEP grid with MM5 forcing. Runoff input is as described in Section 2.1.3.
Case B: To test the effect of the higher resolution surface forcing provided by MM5, 2001 was re-run with NCEP forcing, with the boundary conditions from the NEP grid also run with NCEP forcing.
Case C: To test the influence of tidal mixing, 2001 was re-run as in Case A (including the values for viscosity described in Section 2.1.2), but without tidal forcing.
Case D: To test the effects of brackish river inflow, 2001 was re-run as in Case A, but with freshwater input with zero salinity, input only at the topmost vertical grid-cell.

Case E: As another test of the form of river input, 2001 was re-run with freshwater input of zero salinity as in Case D, but input over a vertical profile which decreases linearly with depth, meant to simulate mixing in estuaries.

For these large modeling experiments, we used the message passing interface (MPI) parallelization option available in ROMS, and the "mpich" MPI implementation. Model runs were performed on a supercomputer of distributed parallel LINUX nodes provided by the Forecast Systems Laboratory in Boulder, CO. On 64 processors, one model year of the CGOA grid took approximately one week of wall-clock time on this system.

2.2. Atmospheric model

Because mesoscale variations in the surface forcing are often both substantial and systematic due to the prominent terrain surrounding the coastal Gulf of Alaska, a nested set (135, 45 and 15 km resolution) of atmospheric simulations using MM5 was developed to investigate the sensitivity of the modeled oceanic flow. Mesoscale numerical weather prediction models such as the MM5 model, when provided with coarse-scale boundary and initial conditions, have been demonstrated to properly account for the effects of mesoscale terrain (Mass et al., 2002; Bromwich et al., 2005; Zagar et al., 2006; Olson et al., 2007).

Our MM5 simulations were carried out with the following physics packages: simple ice microphysics, Kain–Fritsch convective parameterization, the medium range forecast (MRF) planetary boundary layer (PBL) parameterization, a five-layer soil model, and cloud radiative forcing, as in the experiments conducted by Mass et al. (2002). Data from NCEP was used for initial and boundary conditions on the outer-most of three domains, which has a horizontal grid spacing of 135 km. Newtonian relaxation (nudging) was used on the outer-most domain to constrain the solution to closely follow NCEP on the synoptic scale. The simulations were run piecewise in overlapping 48-h blocks; hours 12–48 of each simulation were averaged and written to an output file to provide forcing for the ocean model.

The inner of the three nests used covers the CGOA with a horizontal grid spacing of 15 km. This configuration was selected as a compromise between computational expense and resolution, following the results from Mass et al. (2002) for mesoscale features produced by topography in the Pacific Northwest, and after some experimentation. A grid spacing of 15 km appears to be sufficient to resolve mesoscale coastal phenomena such as barrier jets (Winstead et al., 2006), if not microscale features due to small variations in the terrain.

The MM5 simulations ran independently from the oceanic simulations, and there was no dynamic feedback between them. However, by using the bulk algorithms (Section 2.1.3) to compute the surface sensible and latent heat fluxes for the ocean model, the effect of smaller-scale circulation features on sea-surface temperature are retained for these fluxes. In general, we expect mesoscale variations in winds to have a greater impact on the CGOA's upper ocean than do mesoscale variations in heat fluxes.

No data are available during the winter months, but comparison of the MM5-generated daily averaged wind speed with measured winds at the GAK-3 mid-shelf surface mooring (59.27N, 149.0W) show that the model estimates individual events in the summer and fall accurately (Fig. 3A). Seasonal means are each within $\sim 1\,\mathrm{m\,s^{-1}}$ of their observed values, and R^2 values between model and observation are ~ 0.58 in each season of data (significant at the 1% level). The daily mean MM5 values have less high-frequency variability than the hourly measurements; this may lead to some underestimation of mixing during intense storms.

2.3. Data collection and processing

Model results were validated using in-situ data collected by hydrographic surveys, mooring deployments and drogued drifters. Hydrographic surveys along the Seward Line were performed during 15 LTOP cruises and three mooring maintenance cruises throughout 2001 and 2002; these station locations are marked on Fig. 2. As part of the LTOP program, moorings were also deployed at several Seward stations; this paper makes use of temperature and salinity available for 2001 from the GAK-1 station location (Weingartner et al., 2005).

Stratification in the CGOA is determined mainly by salinity. Given this, plots of salinity are sufficient to characterize the model's replication of the mixed layer for our purposes. To summarize the seasonal variations in stratification measured along the hydrographic sections, we computed the water column potential energy anomaly, ϕ ($\mathrm{J\,m^{-3}}$), which is the amount of energy required to completely mix the water column (Simpson, 1981). This stratification index is useful because it simply illustrates the results of complex processes. For example, it has been used to create an empirical formulation of mixing in an estuary (Garvine and Whitney, 2006). It is defined as

$$\phi = \frac{1}{h}\int_{-h}^{0}(\rho - \bar{\rho})gz\,\mathrm{d}z, \text{ where } \bar{\rho} = \frac{1}{h}\int_{-h}^{0}\rho\,\mathrm{d}z\,.$$

where h is the water column depth in meters or 100 m (whichever is less), ρ is the modeled or measured density of sea water ($\mathrm{kg\,m^{-3}}$) at depth z, and g is gravitational acceleration ($9.81\ \mathrm{m\,s^{-2}}$). To track the seasonal cycle, ϕ was computed for each hydrographic profile along the Seward Line, then averaged across the shelf. Potential energy anomaly was also computed from the model output at grid-points most closely corresponding to the locations of the Seward Line stations.

Calculated transport past Cape Kekurnoi, derived from a cross-strait/depth integral of current meter data, is used to validate the model's replication of the ACC. Because of eddies and variability in the location of the ACC's high speed core, currents are not correlated with local winds, whereas transport is (Stabeno and Hermann, 1996), and along-shore currents are uncorrelated or weakly correlated from Gore Point (on the Seward Shelf) to Cape Kekurnoi (in Shelikof Strait), whereas transport is correlated (Stabeno et al., 1995). From Kayak Island to the Seward Line, the ACC is convoluted, likely because of complex topography (Stabeno et al., 2004), and at Cape Fairfield, where transport estimates are more reliable (Weingartner et al., 2005) there are not the necessary data, so transport is calculated from measurements in Shelikof Strait, rather than on the Seward Shelf. The magnitude of transport is lower at Cape Kekurnoi than at Gore Point, and has more frequent reversals, but these transports are correlated (Stabeno et al., 1995).

From Spring 2001 through Summer 2002, an array of three ADCP current meters was moored along the Cape Kekurnoi line in Shelikof Strait (Fig. 2); distance between moorings is $\sim$18 km, across the 40 km wide strait (Stabeno et al., 2004). Velocities measured by the moorings were rotated to the along-shore frame of references, and filtered with a 35-h Cosine squared Lanczos filter to remove tides and high-frequency variability and sub-sampled 6 hourly. Transport across the Cape Kekurnoi line was calculated by multiplying the downstream velocity by the depth and height sampled by each ADCP bin, summing over each instrument on the mooring, then summing the instruments over the line (Stabeno et al., 1995, 2004). This transport

can be compared to the model-generated transport, which was calculated from the vertically averaged velocity at the model grid-points across the Cape Kekurnoi line. Positive values for transport indicate the current is in the direction of the ACC (roughly westward), and negative values indicate a reversal of the ACC (roughly eastward currents).

Current meters moored along the Gore Point Line (Fig. 2) are used to examine the averages and time-domain EOF structure of along-shore subtidal currents on the Seward Shelf. Eight Aanderaa current meters (four depths at each of two locations; 58.96°N, 150.93°W and 59.11°N, 150.99°W) were deployed for the period May–September, 2001; time series were low-pass filtered and compared with subtidal velocities at the same locations extracted from the model.

Horizontal maps of velocity were derived from approximately 10 years of data from satellite-tracked drifters drogued at ~40 m (Stabeno et al., 2004). All available velocity estimates within 0.5° longitude by 0.25° latitude bins were averaged for summer (May–September) and winter (October–April). Only bins that had at least four independent velocity estimates were included in the map; independence is here defined as being separated by at least 3 days (which is the dominant decorrelation time for subtidal velocities in this region). Observations from waters deeper than 3000 m were excluded, as these are improperly aliased by large, persistent 200-km scale eddies. Equivalent model velocities on the same grid were obtained by temporally averaging over the same summer and winter periods for 2001–2002.

3. Results

3.1. Base case

3.1.1. Seasonality

The CGOA model was spun-up from initial conditions provided by the NEP model. Daily surface kinetic energy averaged over the entire domain (Fig. 4) shows that the energy level of the model is high initially; the average value in January is higher in 2001 than in 2002. Spatially, the initial decrease in surface kinetic energy is most pronounced in the basin (not shown); perhaps the high viscosity which is required to keep tidal velocities stable in the CGOA model (see Section 2.1.2) is also dampening the eddy field that is inherited from the NEP model. Since the adjustment occurs mainly within the first few months, further analysis will be restricted to after March 1, 2001. After that, the lowest surface kinetic energy is in the summer, and fall and winter are dominated by large-magnitude events.

Differences between summer and winter also can be seen in the seasonally averaged velocities at 40 m (Fig. 5). The ACC, which is present along the coast, is stronger in winter. The AS along the shelf-break is often distorted by off-shore eddies, but otherwise shows little seasonal variation. The shallow banks southeast of Kodiak Island have clockwise gyres above them which are stronger in summer than in winter. All these features mirror those found in the drifter-derived maps of currents. In both seasons, the spatial means of modeled N/S and E/W currents are each within $\sim 2\,\mathrm{cm\,s^{-1}}$ of their observed values, and the R^2 of these properties with their measured equivalents are ~0.38 and ~0.54, respectively (both significant at the 1% level).

The average cross-shelf structure of the ACC on the Seward Shelf is well represented by the model. Seasonal averages are shown in Fig. 6A and B. Each shows $\sim 20\,\mathrm{cm\,s^{-1}}$ westward along-shore flows at 30 m depth at the northern mooring, $\sim 10\,\mathrm{cm\,s^{-2}}$ along-shore flow at 30 m at the southern mooring, and vertical shear to near zero values at 140 m depth for each location. The first EOF of both model and data has a pattern similar to the means (Fig. 6C and D), which explains ~60% of the variance of each signal; the time series of the first EOF for the model and data are correlated with an R^2 of 0.37 (significant at the 1% level; Fig. 6E).

3.1.2. Seward line hydrography

Transects of the Seward line were completed in March, April, May, July, August, October and December. We illustrate the seasonal cycle of salinity and temperature using April, August and December transects. Salinity measured during the LTOP cruises (Williams et al., 2007; Childers et al., 2005; Weingartner et al., 2005) show the surface freshwater of the ACC trapped along the coast in spring and early summer (Fig. 7A). However, in the late summer and fall, the surface salinity at the shelf-break (Stations 7–9) can be less than 32 psu as the ACC spreads across the shelf (Fig. 7B). Deep (300 m) off-shore salinity is between 33 and 34 psu, and during the summer, when downwelling relaxes, on-shore flux at depth of higher salinity water onto the shelf has been observed (Childers et al., 2005); at depth, the 33 psu isohaline is farthest off-shore in April, intrudes on-shore in June, and then appears to retreat in winter as freshwater is mixed downward and downwelling favorable winds increase in strength. Instabilities propagating through the region in summer and fall can cause significant salinity signals at inner shelf stations (GAK-2 and -3) in the upper 30 m on scales of 6 days, and these signals may lead to discrepancies between modeled and observed hydrography at these locations.

After some initial adjustment (not shown), the timing and magnitude of the modeled surface freshwater signal matches the data well (Fig. 7D–F). It is trapped along the coast in spring, and extends across the shelf in summer and fall, although the low-salinity layer does not extend quite as deep as observed.

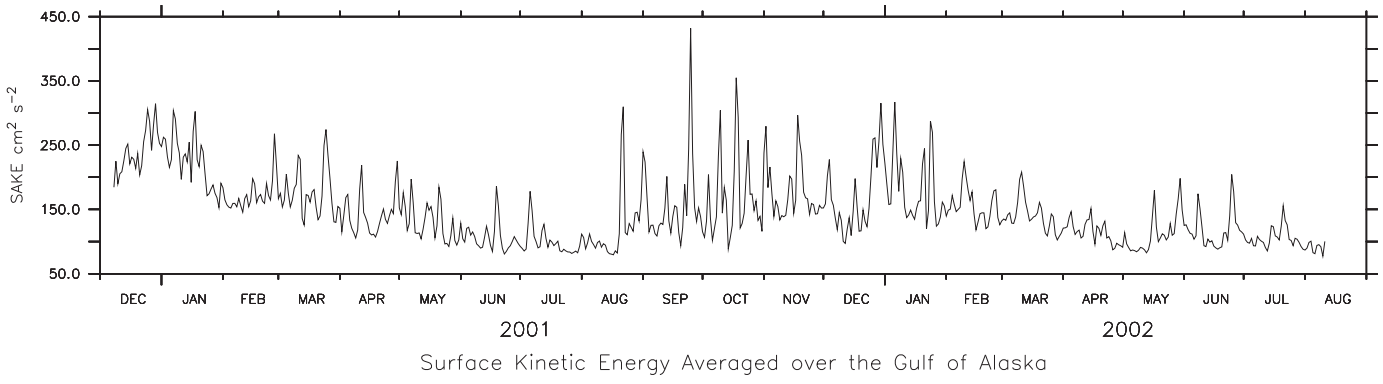

Fig. 4. Surface kinetic energy ($\mathrm{cm^2\,s^{-2}}$) averaged over the model domain.

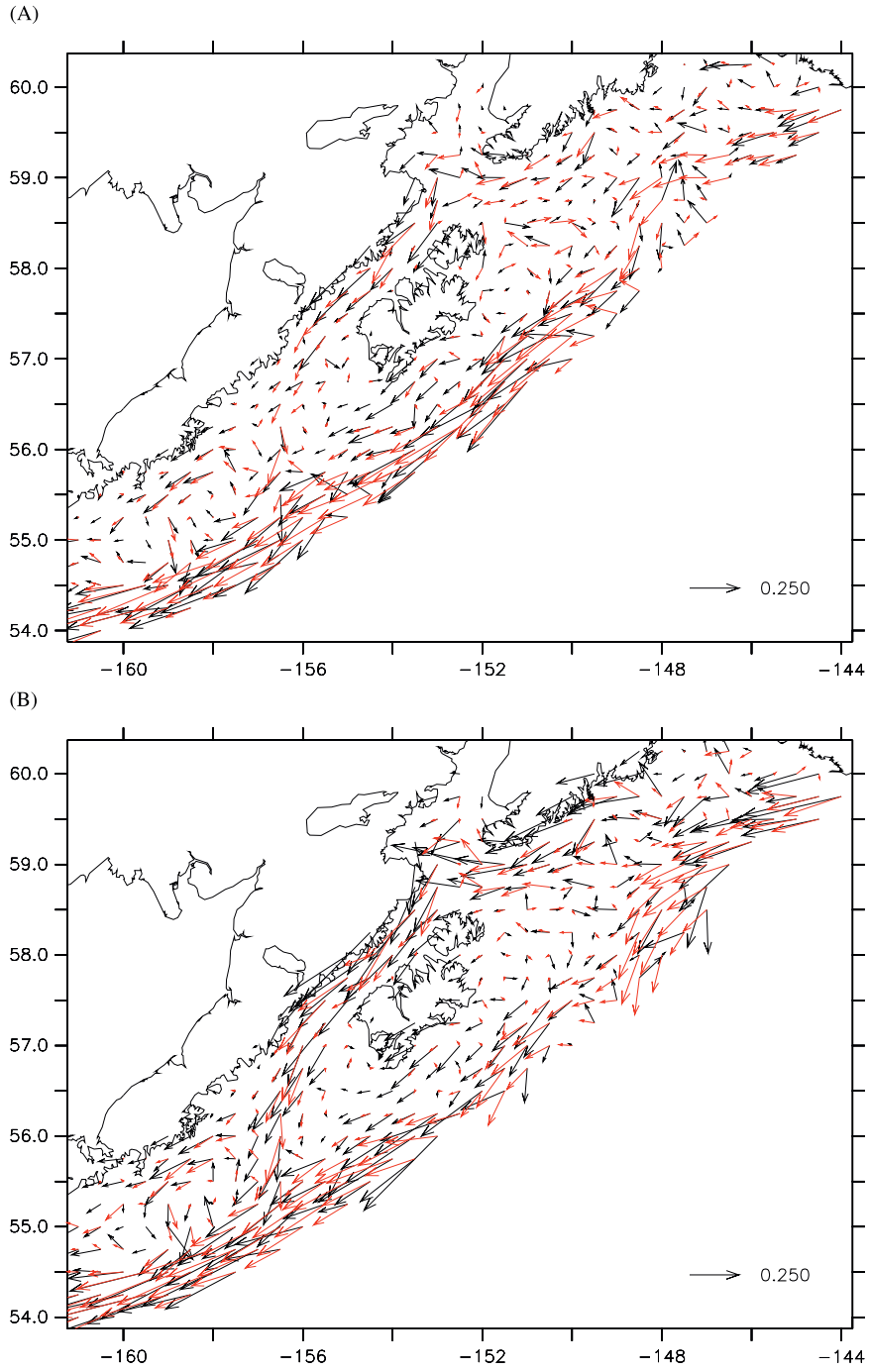

Fig. 5. Mean velocity vectors ($m\,s^{-1}$) at 40 m on the CGOA shelf, computed from drifter data (black) and model (red): (A) summer period (May–September) and (B) winter period (October–April).

Beginning with initialization, the model does less well reproducing deep and off-shore salinity. Although the 33.5 psu isohaline often intersects the shelf-break at the correct depth, modeled surface salinity in the basin is too high by 1–2 psu, with the 33 psu isohaline outcropping over the shelf-break in the winter. A similar discrepancy in salinity was observed in a comparable model of the Bering Sea (Stabeno et al., 2008) and is likely a result of the large-scale Pacific model being too salty. Inshore, modeled salinity deeper than 100 m does exhibit a summer-time increase of approximately the right magnitude, but the 33 psu isohaline never retreats off the shelf. These problems improve as the model run continues into 2002, but are not completely resolved.

The coldest measured temperatures (4 °C) are at deep off-shore locations in April and May, and the highest temperatures (>12 °C) are at the surface across the entire transect in June/July/August (Fig. 8A–C). In 2001, measured temperature inversions of 1–2 °C are widespread above 200 m in March and April, are restricted to particular stations in December and May, and are non-existent in July and October. Modeled temperatures are persistently too cold at the surface, especially in winter, and too warm at depth, leading to larger temperature inversions earlier in the year than are observed (Fig. 8D–F).

Comparison of model results with individual mooring locations is complicated by the model's contraction of the ACC against

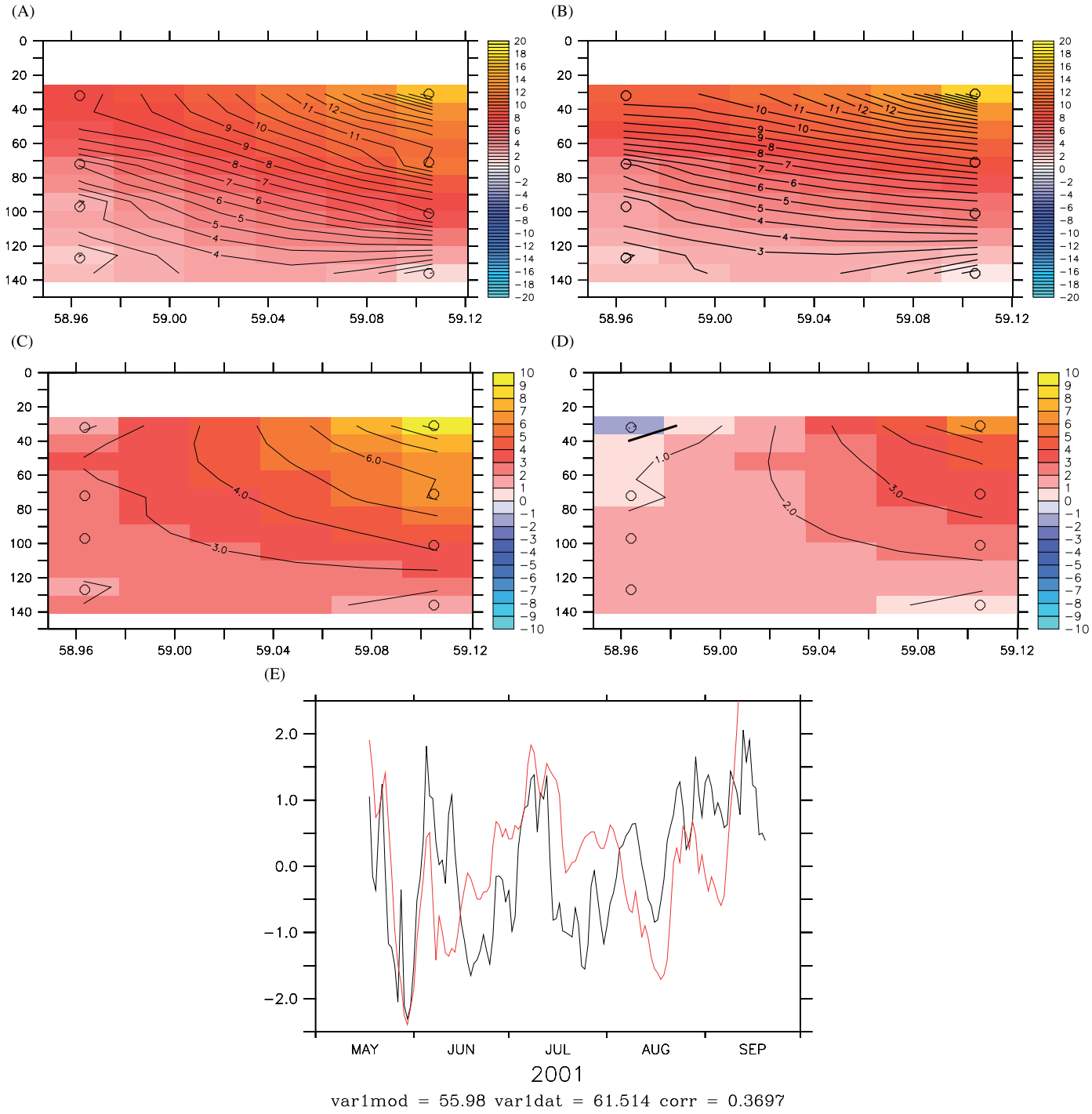

Fig. 6. Along-shore velocity ($cm\,s^{-1}$) at Gore Point moorings (latitude vs. depth): (A) mean summer velocity for data, (B) mean velocity for model, (C) first EOF pattern for data, (D) first EOF pattern for model, and (E) time series for the first EOF for data (black) and model (red). Percent of the variance explained is 56% (model) and 62% (data), and the correlation between the two series is 0.36.

the coast and by the irregular nature of the frontal instabilities which transit the Seward shelf. Stabeno and Hermann (1996) note there was low correlation between measured mesoscale variability and that produced by their model, except in confined regions such as Shelikof Strait. Nevertheless, comparison of measured (Fig. 9) and modeled (Fig. 10) temperature and salinity at GAK-1 during 2001 shows that the model replicates the seasonal ranges for these values. The differences already noted are also present in the time series—namely, the shallow mixed layer, the missing winter-time decrease in salinity at depth, and the erroneous temperature inversions in the model. The differences confirm model weaknesses identified previously, as the effects of instabilities are found too far inshore and too shallow. In the model results, the salinity signals have higher magnitude during relaxations in local downwelling favorable winds (Fig. 3A), and slowing of the ACC (Fig. 12A).

There is considerable variability in the surface salinity. It is usually constrained to grid-points near the coast, but during the periods July 2001 to January 2002 and after August 2002, when runoff is high, the highest temporal variance in surface salinity is 20 km off-shore. The highest variance occurs over and downstream of shallow banks, where the model produces many

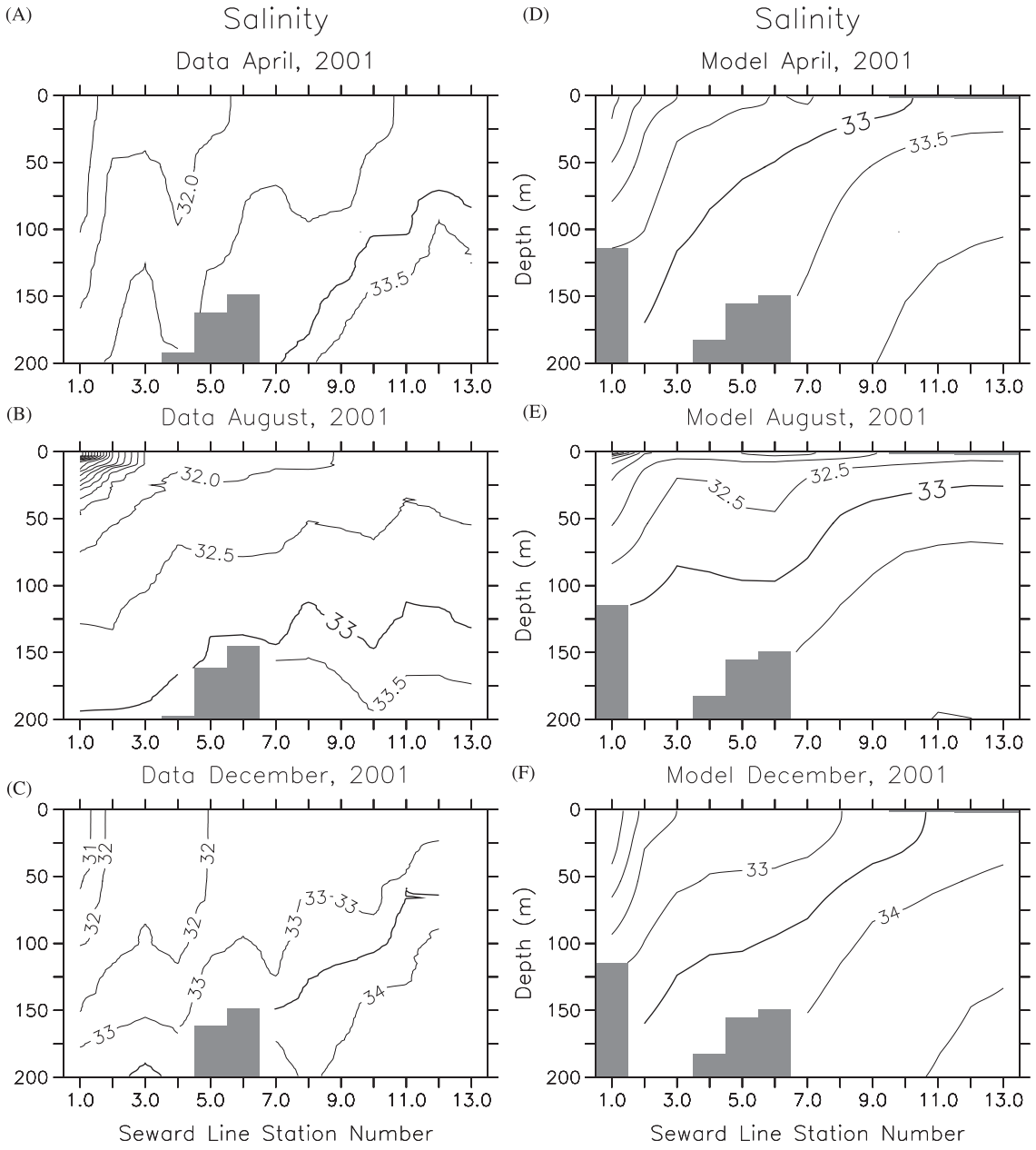

Fig. 7. Salinity from the data (A–C) and model (D–F) along the Seward hydrographic line. Station numbers are 1 (on-shore) to 13 (213 km off-shore). Contour interval is 0.5, and the 33 psu isohaline is denoted with the heavier black line. Data were collected April 4–7, July 31–August 2, and December 7–11, 2001, and modeled values are averaged over the entire month.

meanders and eddies in the ACC (Fig. 11A). Individual meanders are not coherent farther than 60 km downstream, and travel this distance in 4–8 days, with a phase speed of 9–15 cm/s. Surface salinity increases as the ACC passes through Kennedy and Stevenson Entrances, where there is high vertical mixing (K_t, Fig. 11B). This disruption of the surface signature of the ACC at Kennedy and Stevenson Entrances has been observed historically (Stabeno et al., 2004) and using surface measurements obtained by instruments mounted on a ferry boat (E. Cokelet, pers. comm).

3.2. Data indices

The seasonal features of the ACC are summarized by its transport, but transport over the Seward shelf is difficult to define because of the complex topography and meanders in the ACC. Instead, Cape Kekurnoi, downstream in Shelikof Strait, offers a convenient place to calculate the transport of the ACC (Fig. 12A). The measured transport there has strong variability at high frequencies (days), with changes of almost 2 Sv over just a few days. It is highest between November 2001 and February 2002 (1.2 Sv), followed by a sharp drop off in March, 2002. Low or negative values characterize July and August in both years, and April and May of 2002. Analysis of the velocity profiles shows that the current is intensified on the mainland side and is weaker or reversed on the Kodiak Island side, without much surface intensification.

The magnitude of the modeled ACC transport matches the measured transport very well, but variability is underestimated at all time scales. Modeled events correspond to real events even on a daily time scale, though at reduced intensity. The seasonal signal is also underestimated in the model; transport is too high in

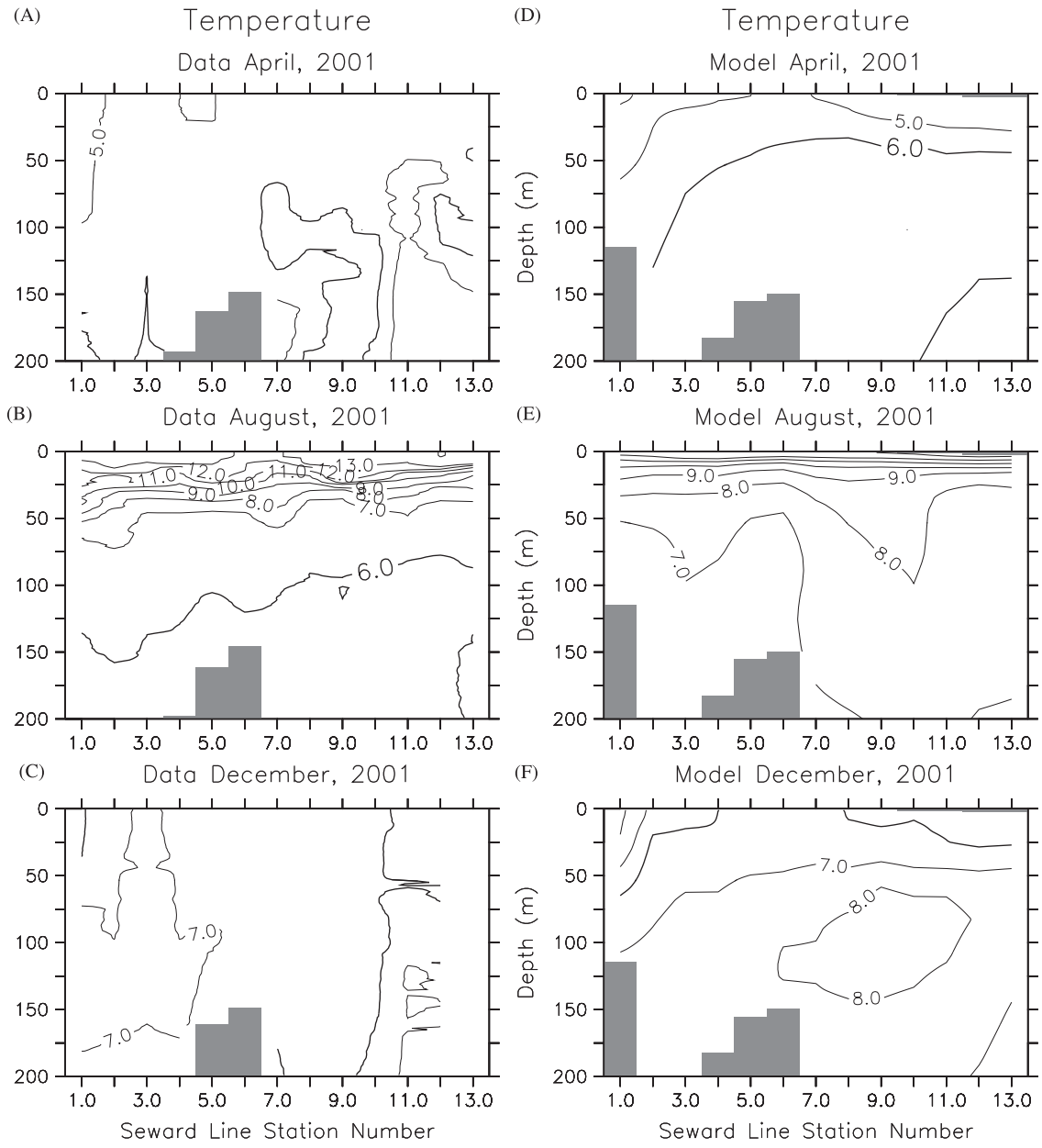

Fig. 8. Temperature (°C) from the data (A–C) and model (D–F) along the Seward hydrographic line. Station numbers are 1 (on-shore) to 13 (213 km off-shore). Contour interval is 1 °C, and the 6 °C isotherm is denoted with the heavier black line. Data were collected April 4–7, July 31–August 2, and December 7–11, 2001, and modeled values are averaged over the entire month.

summer and too low in winter, and the transition in spring, 2002, is not sharp enough. Modeled currents are surface intensified, and there are few reversals in the current, even along Kodiak Island. The lack of current reversals in the model reduces the fit during the summer period; the R^2 of the linear regression of modeled transport to measured transport is 0.59 in the winter (September 2001–May 2002), but only 0.39 in the summer (May 2001–September 2001) (both significant at the 1% level). While some of this discrepancy is due to the model, the observations also contribute to it. Transport was calculated with only three moorings, which is the minimum number that could be used to provide reliable estimates of transport.

Potential energy anomaly, ϕ calculated from hydrographic surveys along the Seward Line shows the lowest stratification from December through May, and the highest from July through October (Fig. 12B). These changes reflect the seasonal evolution of the ACC; in April, it is steep and narrow (<10 km), in August, it is wide (30–50 km) and shallow (50 m), and in December, it is wide (30 km) and deep ($\sim$100 m) (Williams et al., 2007; Weingartner et al., 2005). The model also produces this seasonal pattern, but, again, the seasonal variability is not strong enough. Correspondence is worst in the winter and early spring, when the model does not produce enough vertical mixing. ϕ in summer might be underestimated due to the model's ACC being trapped closer to the coast than it is in reality.

Fig. 12C summarizes the seasonality of the ACC transport and potential energy anomaly indices from observations and the model. Both have been filtered with a 30-day running mean to emphasize the seasonal signal. It is clear that the model occupies a more restricted space in this plot, illustrating the reduced

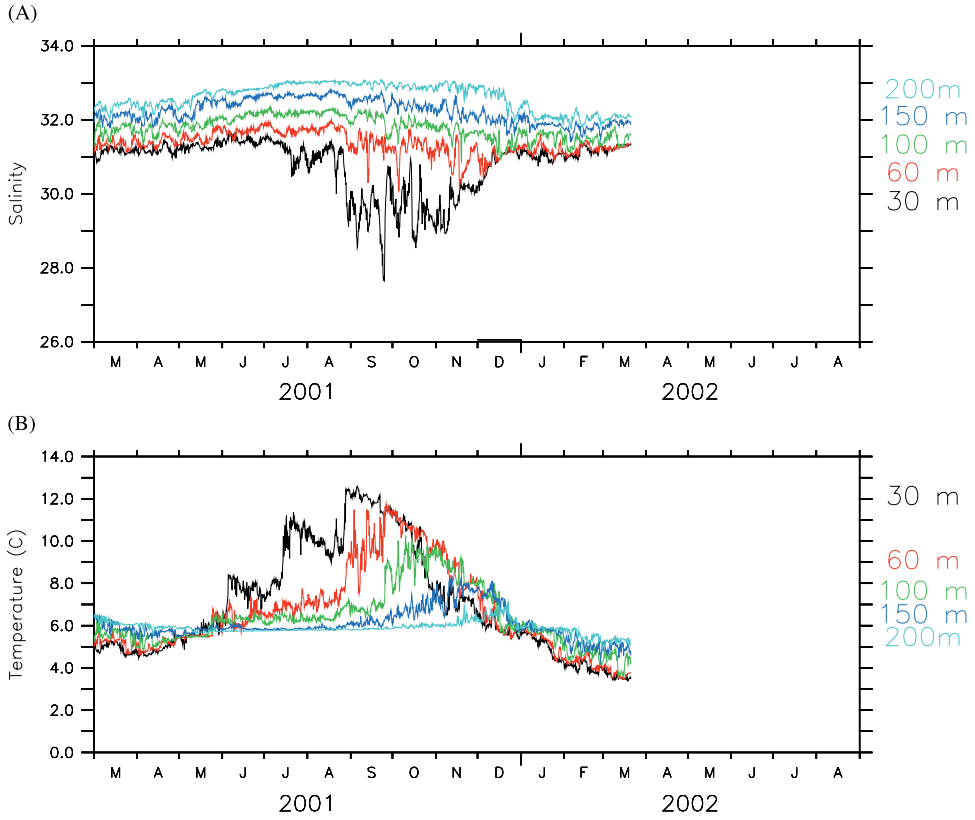

Fig. 9. (A) Salinity and (B) temperature (°C) measured by the mooring located at the GAK-1 station location, the innermost Seward line station. Depths from 30 to 200 m are color coded. Data provided by T. Weingartner (University of Alaska, Fairbanks).

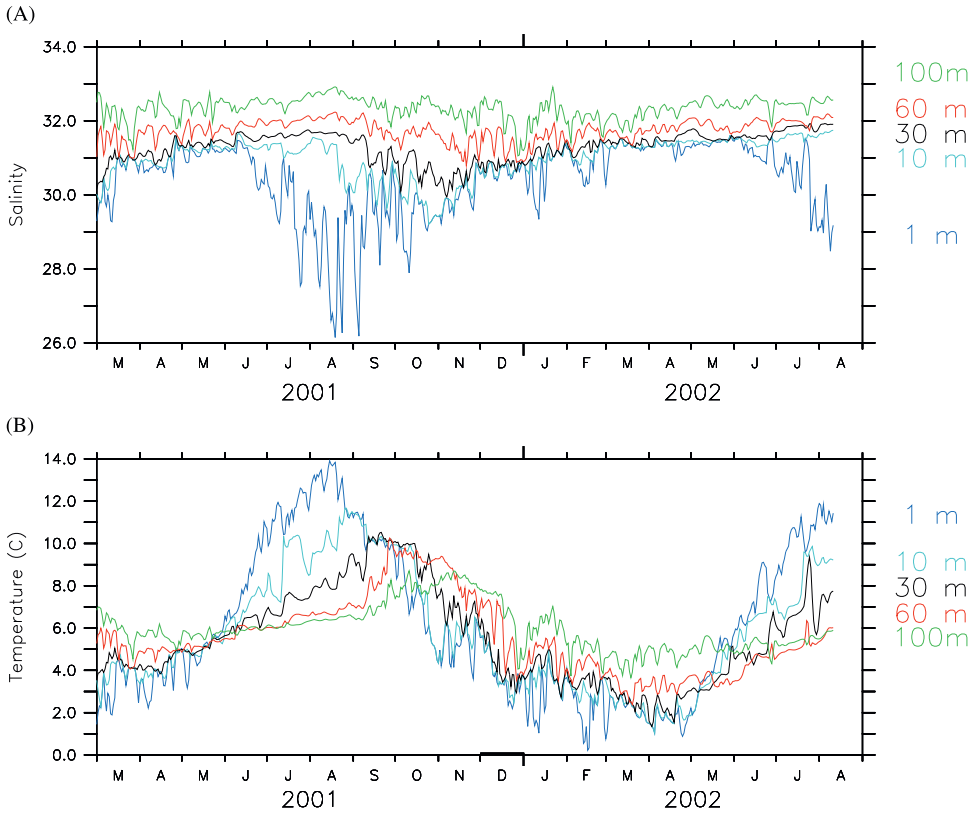

Fig. 10. (A) Salinity and (B) temperature (°C) extracted from the model results at the GAK-1 mooring location, the innermost Seward line station. Depths from 1 to 100 m are color coded. Note: model bathymetry is not as deep as real bathymetry at GAK-1.

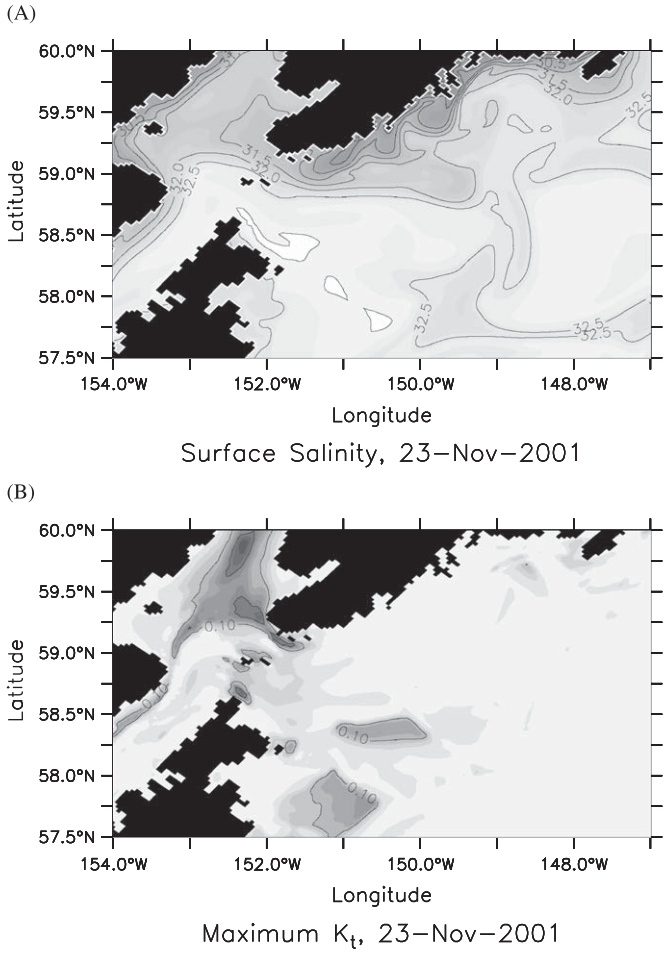

Fig. 11. (A) Surface salinity (contour interval 0.5) and (B) maximum vertical diffusivity (K_t, contour interval 0.1 $m^2 s^{-1}$) on the Seward shelf on November 23, 2001 from the model.

seasonal signal especially in potential energy anomaly. This type of plot will be useful in the next section, where the results of many different model runs are compared using these data indices.

3.3. Sensitivity tests

3.3.1. Case B: lower resolution (NCEP) surface forcing

In Case B, 2001 was re-run with NCEP forcing, and the boundary conditions came from the NEP grid which was also run with NCEP forcing (Hermann et al., 2009a). The results occupy a smaller region in the data indices space than Case A's results do (Fig. 13A). This translates to slightly lower vertical stratification in the summer, and lower ACC transport at all times, but particularly in the fall and winter. In the NCEP dataset, winds are oriented less strongly along-shore due to smoother topography and hence reduced orographic steering (Stabeno et al., 2004). The modeled result is a weaker ACC, as expected. However, the minimum values of surface salinity on the shelf (Fig. 14A) are almost indistinguishable from those produced by Case A (not shown).

3.3.2. Case C: no tidal forcing

In this case, the model was run with the original MM5 forcing, but tidal forcing was removed. Stratification is approximately equal to that of Case A, but the transport is greatly increased (Fig. 13B). Since stratification at Seward is relatively unchanged, we can infer that tidal mixing has little effect on the stratification there; this makes sense looking at the locations of high K_t in Fig. 11B. Mixing is high in Stevenson and Kennedy Entrances, near Cook Inlet, which apparently disrupts the flow continuing on into Shelikof Strait. This is illustrated by comparing the minimum surface salinity generated by Case B (Fig. 14A) with that of Case C (Fig. 14B); the latter shows less disruption in the low surface salinity values at Stevenson Entrance. Without tidal mixing in the passes, the buoyancy-driven flow apparently can continue relatively unimpeded to Cape Kekurnoi.

3.3.3. Case D: freshwater input at the surface only

Our use of brackish water in the river runoff in the Base Case is non-standard compared to other modeling efforts (H. Arango, pers. comm.). A common way to introduce river runoff is with water of zero salinity input only to the topmost grid-cell. However, in the CGOA configuration, with large amounts of freshwater input into estuaries which are not resolved by the model, this method did not work. Stratification on the shelf increases to values far higher than measured, leading the model to crash in late summer (Fig. 13C). Low-salinity water occupies much more of the surface shelf than is realistic (Fig. 14C).

3.3.4. Case E: freshwater distributed vertically

Case E is 2001 run with the Alaskan line-source's freshwater input defined to have zero salinity, with a vertical volume profile that decreases linearly with depth in order to simulate mixing in coastal estuaries. As in Case D, this case has higher than measured stratification (Fig. 13D), which occurs as freshwater spreads farther across the shelf than is observed (Fig. 14D). This surface freshwater does not get mixed down in the winter. The change in the vertical structure of freshwater input does not affect transport past Cape Kekurnoi (Fig. 13D).

4. Discussion

The CGOA model's shallower than expected mixed layer and persistent temperature inversions might be the result of lower than realistic vertical mixing. Insufficient vertical mixing could also impact the observed on-shore movement of the 33 psu isohaline in summer. Williams (2003) suggested that this movement is not dependent on upwelling windstress, but instead is the result of reduced production of intermediate water (<33 psu) when wind mixing decreases in summer. Intermediate water is continually transported along the shelf by the ACC, and if it is not being replaced by mixing, then the volume enclosed by the isopycnal decreases, and the isopycnal moves on-shore. If our model lacks sufficient seasonal variation in wind mixing, that would explain why it does not generate enough movement in this isopycnal, even though the model's ACC transport is approximately correct.

The model's sensitivity tests hint at what might improve this situation. Neither the addition of tidal mixing nor the use of higher resolution winds sufficiently improved the stratification, as measured by potential energy anomaly. Instead, the salinity of the input line-source clearly had the greatest effect. Clearly, there is room for improvement in the form of the input line-source, perhaps by using data assimilation techniques or by employing a box model to process the freshwater before it is added to the coast (Garvine and Whitney, 2006). It is interesting to note that significantly different versions of stratification generated by the various runoff scenarios are all associated with good replication of along-shore transport through Shelikof Strait. This is consistent with the results of Hermann and Stabeno (1996), which suggested that the ACC transport is affected more by changes in wind stress

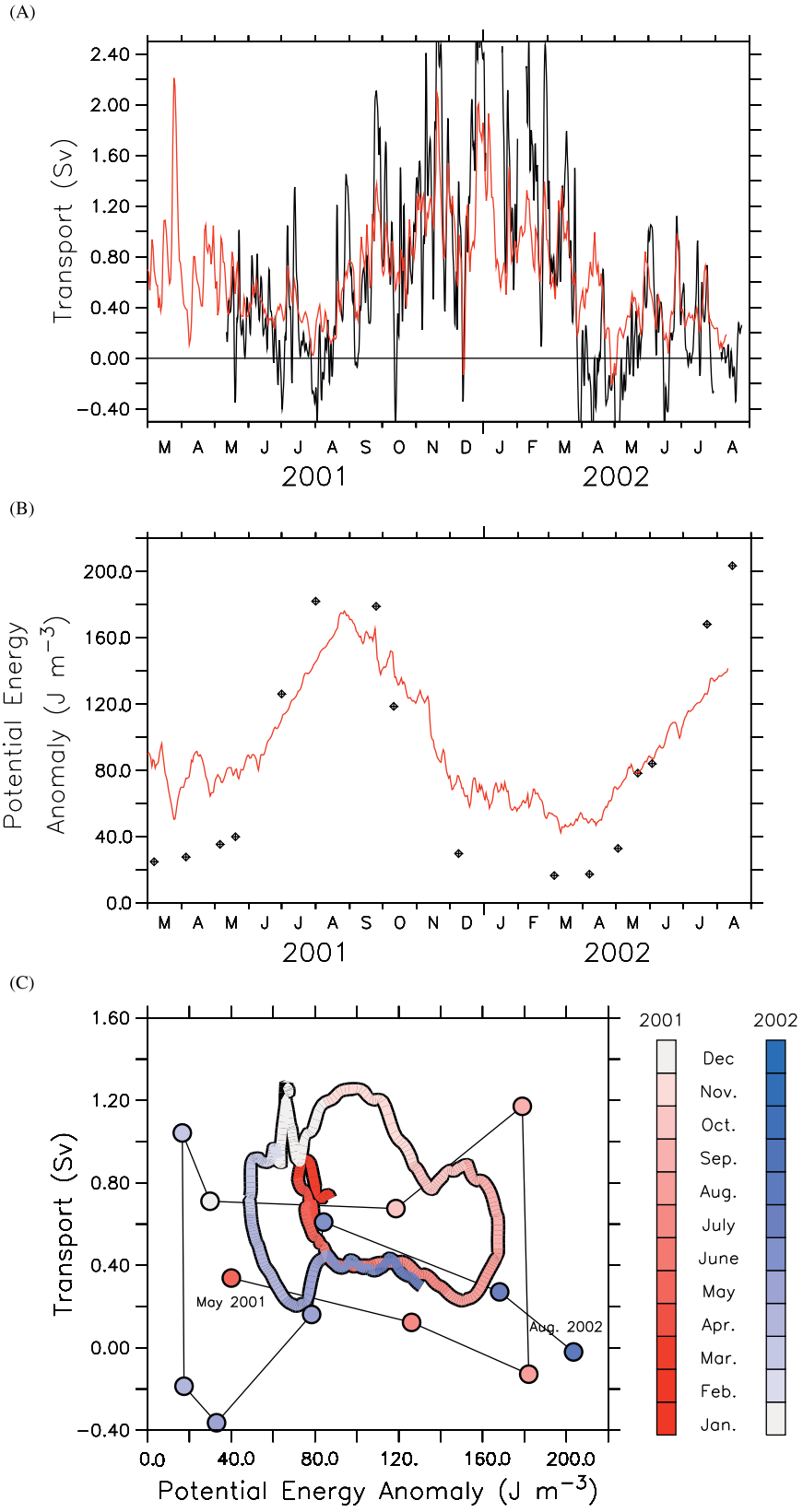

Fig. 12. (A) Transport through Shelikof Strait. Modeled transport is the red line, measured is black. (B) Potential energy anomaly (ϕ) averaged across all available stations on the Seward hydrographic line. Modeled ϕ is the red line, and measured are the black dots. (C) Transport plotted against ϕ for data (dots) and model (shaded line), color coded by time of measurement. Both are filtered with 30-day running mean.

than by changes in buoyancy forcing. Williams (2003) also found that freshwater transport in the ACC is independent of cross-shelf structure.

The main problem is that in the CGOA, the deep, narrow fjords that feed the line-source are not resolved by our 3-km grid resolution, and, in essence, the estuary has been moved out onto

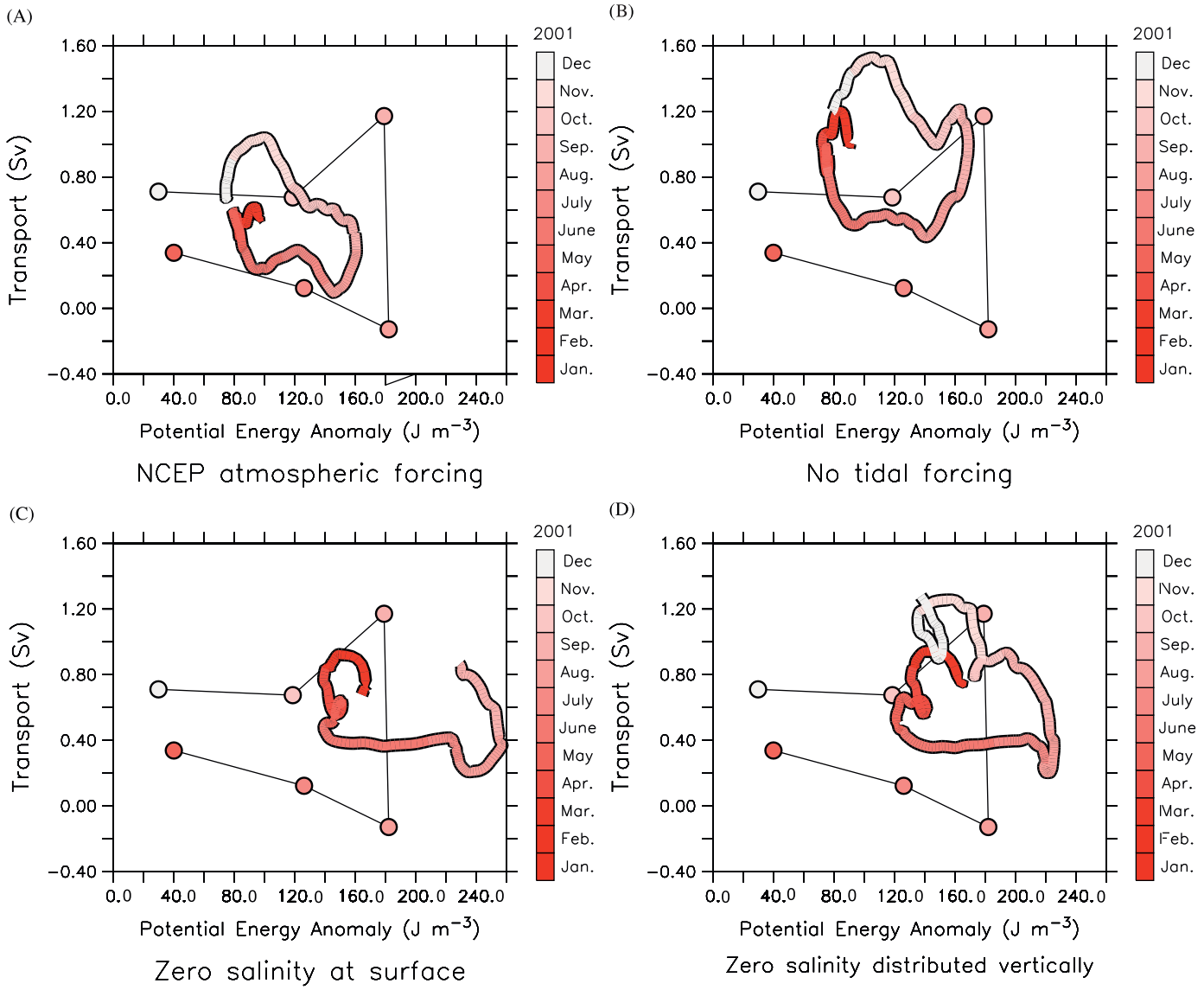

Fig. 13. Transport through Shelikof Strait plotted against potential energy anomaly (ϕ), and colored by the time of measurement. Data is dots and model is shaded line: (A) model forced with NCEP atmospheric variables, (B) model without tidal forcing, (C) model forced with freshwater input along the line source with zero salinity, input at the top-most vertical grid-cell only, and (D) model forced with freshwater input along the line source with zero salinity, input over a vertical profile.

the shelf. This is an extremely difficult test for a mixing scheme. It has been noted that the KPP mixing scheme does not mix as much as the Mellor–Yamada mixing scheme (Mellor and Yamada, 1974, 1982) does in the presence of stratification (Durski et al., 2004), so our decision to keep the KPP mixing scheme consistent from basin to regional scales may have had an unfortunate consequence on the Seward Shelf. However, a comparison of several mixing schemes, including Mellor–Yamada, using a 1D model of an estuary found that none of the schemes could simultaneously (a) allow enough stratification over diurnal periods, and (b) restore mixed conditions following accumulation of stratification during neap tides, leading to "runaway" stratification (Vaz and Simpson, 1994).

It is also possible that the physical configuration of a numerical model can generate unusual cross-shelf and up-shelf transport in the river plumes of single point sources (Garvine, 2001). A steep bottom slope, rectangular inlet shape, unrealistic density profile, and high coastal wall all contributed to development of modeled plumes which spread quickly off-shore, unlike those observed in nature. Given a plume of this type, the vertical closure scheme affects the plume's water mass structure more than grid resolution or advection scheme, but it will not correct the fundamental form of the plume (Hetland, 2005). Previous models of line-sources appear to have similar issues. Off-shore transport at the upstream end, or head, of a line-source produced a bulge of lower salinity water in its plume region (Kourafalou et al., 1996), although it is possible to avoid the production of a similar bulge by beginning the line-source with an along-shore ramp of the inflow volume (Williams et al., 2007). The CGOA has steep bathymetry, and a coastal wall of 10–300 m because of the filtered bathymetry, so some of these configuration issues might apply. However, the head of the line-source is south of the grid's southeast boundary, and the along-shore locations with the deepest coastal wall do not seem to be areas with consistent off-shore freshwater transport, so how configuration issues apply is not clearly evident.

5. Conclusion

Overall, the model does a good job of simulating conditions over the Seward Shelf in the Gulf of Alaska. This CGOA model

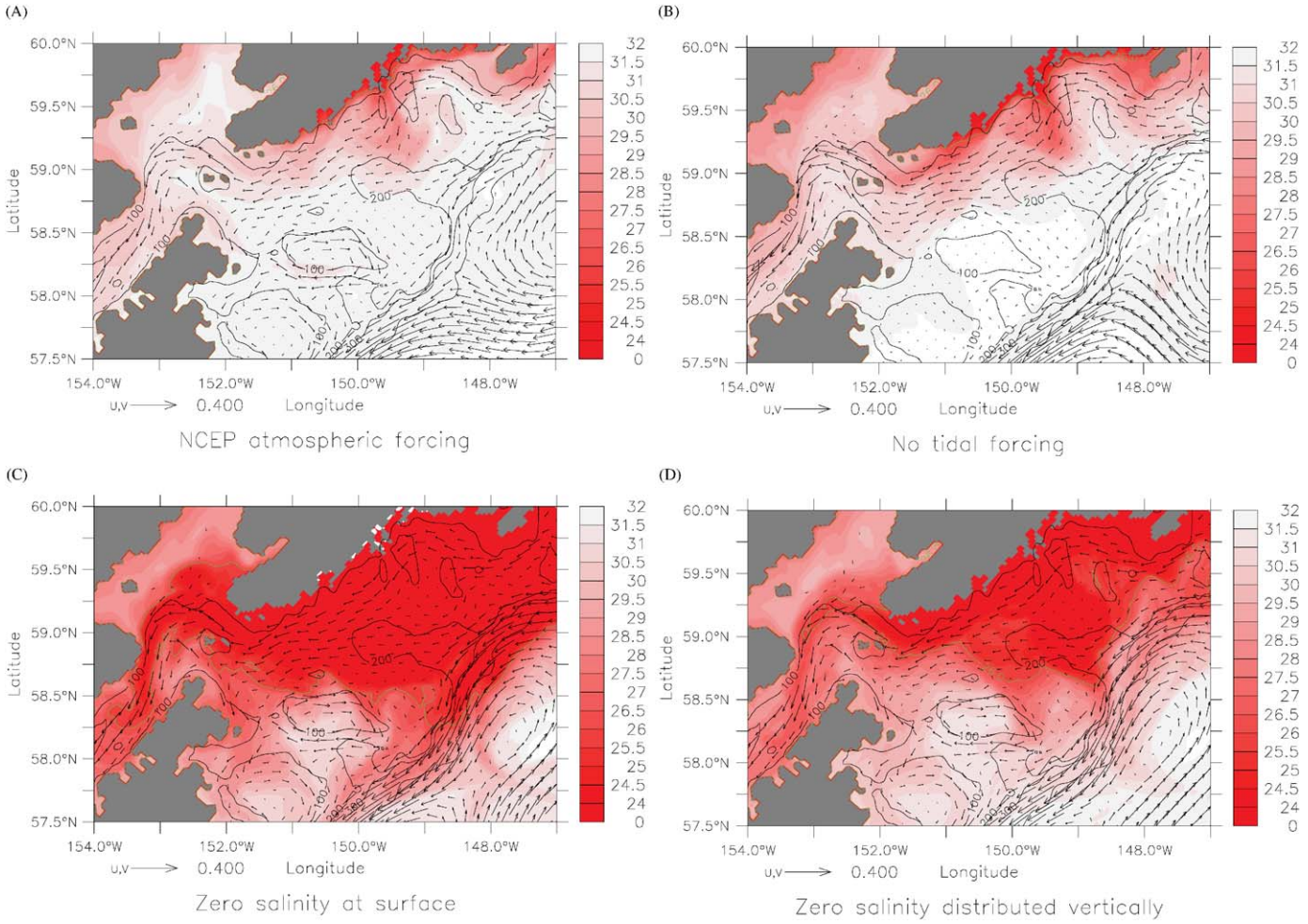

Fig. 14. Minimum surface salinity produced by each model run (shaded) with time-averaged velocity vectors at 40 m depth. Time period is May 1, 2001–September 1, 2001. Bathymetry is in black contours, and the 26 psu isohaline is in green. Model runs are as in Fig. 7.

represents a considerable improvement over previous model results presented in Hermann et al. (2002). The parallel ROMS code and super-computers allowed an increase in grid resolution which strengthened the ACC and AS, increased transport through Shelikof Strait, and improved the cross-shelf structure along the Seward line. There is also much more temporal variability in the newer model results than in previous results, with abundant eddies and mesoscale variability which mimics what has been observed. Time series of salinity and temperature are qualitatively similar to those measured at moorings.

The model produces distinct on-shore and off-shore regimes with a meandering transition zone and appropriate seasonal variations. Hinckley et al. (2009) show that the physics of this model can create distinct coastal and oceanic ecosystems when the effects of iron are included in an nutrient, phytoplankton, zooplankton (NPZ) model. This will be useful when evaluating recent hypotheses regarding cross-shelf structure and productivity in the CGOA. However, interactions between the on-shore and off-shore regimes, as characterized by meanders in the ACC, should be treated as imprecise. The time/space scales of the model's ACC meanders differ from those observed, and the modeled meanders are not as coherent along the shelf as the observed ones are (Stabeno et al., 2004).

The model produces a mixed layer that is generally too shallow, but with appropriate seasonal variations in vertical structure. Stratification (as determined by salinity) decreases in the winter and spring, and strengthens in the summer. Although the too shallow mixed layer will limit the availability of nutrients at the surface, a biological model coupled with these physics was able to simulate the spring phytoplankton bloom and spatial patterns on the Seward shelf (Hinckley et al., 2009). Of concern are the erroneously persistent temperature inversions in spring which will complicate interpretation of the biological dynamics that are temperature-dependent. Despite these biases, the physical model replicates the primary spatial and temporal features of the area, and hence provides a framework for examining nutrient (Hermann et al., 2009b) and biological (Hinckley et al., 2009) dynamics on the CGOA shelf.

The assumption implicit in using an array of nested grids is that the smallest-scale CGOA grid would inherit all the good qualities of the larger grids (spun-up current systems complete with El Niño signals), while deficiencies in the inherited fields should be compensated for by the improved physics allowed by the CGOA domain's increased resolution. This appears to be only partly true. The CGOA model does spin-up quickly, but surface salinities off the shelf remain 1 psu too high, and temperature at 100 m on the shelf remains 2 °C too warm at the end of the 1.5-year run. The NPAC model was run without coastal freshwater runoff; salinities and temperatures in the Gulf drift (depart) from expectations (i.e. relative to Levitus) in the NPAC run. Moreover, salinity off the shelf is persistently greater than expected throughout the 7-year spin-up of the NEP domain. However,

interannual features such as equatorially-originating El Niño are generated in the basin-scale domain and passed to the intermediate-scale NEP grid (Hermann et al., 2009a) The nested-grid scheme remains valuable since one of the goals of the nesting scheme is to investigate how larger, climate-scale phenomena modify CGOA features such as the ACC and basin-scale eddies.

As with most modeling studies, improved model runs are already underway. Deficiencies in shortwave radiation are being addressed by the use of corrected interannual atmospheric forcing developed by NOAA's Geophysical Fluid Dynamics Laboratory in support of the Clivar Working Group of Ocean Model Development (WGOMD) Coordinated Ocean Reference Experiments (CORE) (Large and Yeager, 2004); shortwave radiation in that dataset is corrected with data from the International Satellite Cloud Climatology Project (ISCCP). Initial conditions will be improved by including freshwater forcing with all grids, including NPAC, which will hopefully reduce biases in the initial salinity field. The phasing of the CGOA's tidal components has been corrected so that accurate tides at specific times and places can now be generated by this model. In addition, future studies will employ newly developed adjoint techniques to quantify the sensitivity of the circulation and biology to atmospheric and remote oceanic forcing. Testing of other mixing schemes may also be needed to identify the one that works best with the CGOA's high-volume line-source and compensates for unresolved phenomena such as breaking of internal tides. We are presently testing the effects of adding small uniform background mixing to the KPP algorithm, as well as the addition of mixing driven by surface swell (via Langmuir cells).

Acknowledgements

We thank D. Kachel at PMEL for tidal and data analysis and Dr. K. Hedström at UAF for help with ROMS coding. We thank fellow GLOBEC researchers for their helpful comments regarding model development, and for collecting and making their data available for model validation. Specifically, we thank Dr. T. Royer for providing the runoff time series, and Dr. T. Weingartner and S. Danielson for providing mooring data at GAK-1. Dr. K. Coyle suggested using the water column potential energy anomaly as an index that is biologically useful. Dr. S. Hinckley provided helpful comments on early manuscript drafts. We thank the High Performance Computing System at the NOAA Forecast Systems Laboratory in Boulder, CO, for technical help and the allocation on the supercomputer which we used to run the model. We also appreciate the thoughtful comments by two anonymous reviewers, which helped improve this manuscript. This is contribution EcoFOCI-G714 to the Fisheries Oceanography Coordinated Investigations; 1750 to the Joint Institute for the Study of Atmosphere and Ocean, University of Washington; 3128 to the Pacific Marine Environmental Laboratory, NOAA; and 627 to the U.S. GLOBEC program, jointly funded by the National Science Foundation and National Oceanic and Atmospheric Administration. Primary funding for this work was provided by the National Science Foundation Grants OCE00- 02893, OCE-0113461 and OCE-0435592.

References

Beckmann, A., Haidvogel, D.B., 1993. Numerical-simulation of flow around a tall isolated seamount. Part 1: problem formulation and model accuracy. J. Phys. Oceanogr. 23, 1736–1753.

Boyd, P.W., Muggli, D., Varela, D., Goldblatt, R.H., Chretien, R., Orians, K.J., Harrison, P.J., 1996. *In vitro* iron enrichment experiments in the NE subarctic Pacific. Mar. Ecol.-Prog. Ser. 136, 179–193.

Bromwich, D.H., Bai, L.-S., Bjarnason, G.G., 2005. High resolution regional climate simulations over Iceland using Polar MM5. Mon. Weather Rev. 133, 3527–3547.

Chapman, D.C., 1985. Numerical treatment of cross-shelf open boundaries in a barotropic coastal ocean model. J. Phys. Oceanogr. 15, 1060–1075.

Chen, C.S., 2000. A modeling study of the episodic cross-frontal water transport over the inner shelf of the South Atlantic Bight. J. Phys. Oceanogr. 30, 1722–1742.

Childers, A.R., Whitledge, T.E., Stockwell, D.A., 2005. Seasonal and interannual variability in the distribution of nutrients and chlorophyll-*a* across the Gulf of Alaska shelf: 1998–2000. Deep-Sea Res. Pt. II 52, 193–216.

Curchitser, E.N., Haidvogel, D.B., Hermann, A.J., Dobbins, E.L., Powell, T.M., Kaplan, A., 2005. Multi-scale modeling of the North Pacific Ocean I: assessment and analysis of simulated basin-scale variability (1996–2003). J. Geophys. Res. 110, C11021.

Dudhia, J., 1993. A nonhydrostatic version of the Penn State-NCAR mesoscale model: validation tests and simulation of an Atlantic cyclone and cold front. Mon. Weather Rev. 121, 1493–1513.

Durski, S.M., Glenn, S.M., Haidvogel, D.B., 2004. Vertical mixing schemes in the coastal ocean: comparison of the level 2.5 Mellor–Yamada scheme with an enhanced version of the K profile parameterization. J. Geophys. Res.-Oceans 109, C01015.

Fairall, C.W., Bradley, E.F., Rogers, D.P., Edson, J.B., Young, G.S., 1996. Bulk parameterization of air–sea fluxes for tropical ocean global atmosphere coupled ocean response experiment. J. Geophys. Res.-Oceans 101, 3747–3764.

Feely, R.A., Massoth, G.J., Landing, W.M., 1981. Major- and trace-element composition of suspended matter in the north-east Gulf of Alaska: relationships with major sources. Mar. Chem. 10, 431–453.

Flather, R.A., 1976. A tidal model of the northwest European continental shelf. Mem. Soc. R. Sci. Leige 10, 141–164.

Foreman, M.G.G., Crawford, W.R., Cherniawsky, J.Y., Henry, R.F., Tarbotton, M.R., 2000. A high-resolution assimilating tidal model for the Northeast Pacific Ocean. J. Geophys. Res.-Oceans 105, 28629–28651.

Garvine, R.W., 2001. The impact of model configuration in studies of buoyant coastal discharge. J. Mar. Res. 59, 193–225.

Garvine, R.W., Whitney, M.M., 2006. An estuarine box model of freshwater delivery to the coastal ocean for use in climate models. J. Mar. Res. 64, 173–194.

Gill, A.E., 1982. Atmosphere–ocean Dynamics. Academic Press, New York, 662pp.

Haidvogel, D.B., Arango, H.G., Hedstrom, K., Beckmann, A., Malanotte-Rizzoli, P., Shchepetkin, A.F., 2000. Model evaluation experiments in the North Atlantic Basin: simulations in nonlinear terrain-following coordinates. Dynam. Atmos. Oceans 32, 239–281.

Hermann, A.J., Curchitser, E.N., Dobbins, E.L., Haidvogel, D.B., 2009a. A comparison of remote versus local influence of El Niño on the coastal circulation of the Northeast Pacific. Deep-Sea Research II 56 (24), 2427–2443.

Hermann, A.J., Haidvogel, D.B., Dobbins, E.L., Stabeno, P.J., 2002. Coupling global and regional circulation models in the coastal Gulf of Alaska. Prog. Oceanogr. 53, 335–367.

Hermann, A.J., Hinckley, S., Dobbins, E.L., Haidvogel, D.B., 2009b. Quantifying cross-shelf and vertical nutrient flux in the Gulf of Alaska with a spatially nested, coupled biophysical model. Deep-Sea Research II 56 (24), 2474–2486.

Hermann, A.J., Stabeno, P.J., 1996. An eddy-resolving model of circulation on the western Gulf of Alaska shelf.1. Model development and sensitivity analyses. J. Geophys. Res.-Oceans 101, 1129–1149.

Hetland, R.D., 2005. Relating river plume structure to vertical mixing. J. Phys. Oceanogr. 35, 1667–1688.

Hinckley, S., Coyle, K.O., Gibson, G., Hermann, A.J., Dobbins, E.L., 2009. A biophysical NPZ model with iron for the Gulf of Alaska: reproducing the differences between an oceanic HNLC ecosystem and a classical northern temperate shelf ecosystem. Deep-Sea Research II 56 (24), 2520–2536.

Kalnay, E., Kanamitsu, M., Kistler, R., Collins, W., Deaven, D., Gandin, L., Iredell, M., Saha, S., White, G., Woollen, J., Zhu, Y., Leetmaa, A., Reynolds, R., Chelliah, M., Ebisuzaki, W., Higgins, W., Janowiak, J., Mo, K.C., Ropelewski, C., Wang, J., Jenne, R., Joseph, D., 1996. The NCEP/NCAR 40-year reanalysis project. Bull. Am. Meteorol. Soc. 77, 437–471.

Kistler, R., Kalnay, E., Collins, W., Saha, S., White, G., Woollen, J., Chelliah, M., Ebisuzaki, W., Kanamitsu, M., Kousky, V., van den Dool, H., Jenne, R., Fiorino, M., 2001. The NCEP-NCAR 50-year reanalysis: monthly means CD-ROM and documentation. Bull. Am. Meteorol. Soc. 82, 247–267.

Kourafalou, V.H., Oey, L.Y., Wang, J.D., Lee, T.N., 1996. The fate of river discharge on the continental shelf. 1. Modeling the river plume and the inner shelf coastal current. J. Geophys. Res.-Oceans 101, 3415–3434.

Ladd, C., Bond, N.A., 2002. Evaluation of the NCEP/NCAR reanalysis in the NE Pacific and the Bering Sea. J. Geophys. Res.-Oceans, 107, 3158.

Ladd, C., Kachel, N.B., Mordy, C.W., Stabeno, P.J., 2005a. Observations from a Yakutat eddy in the northern Gulf of Alaska. J. Geophys. Res.-Oceans 110, C03003.

Ladd, C., Stabeno, P., Cokelet, E.D., 2005b. A note on cross-shelf exchange in the northern Gulf of Alaska. Deep-Sea Res. Pt. II 52, 667–679.

Ladd, C., Crawford, W.R., Harpold, C.E., Johnson, W.K., Kachel, N.B., Stabeno, P.J., Whitney, F., 2009. A synoptic survey of young mesoscale eddies in the Eastern Gulf of Alaska. Deep-Sea Research II 56 (24), 2460–2473.

Laevastu, T., 1960. Factors affecting temperature of the surface layer of the sea. Comment. Phys.-Math. 25, 1–136.

Large, W.G., McWilliams, J.C., Doney, S.C., 1994. Oceanic vertical mixing—a review and a model with a nonlocal boundary-layer parameterization. Rev. Geophys. 32, 363–403.

Large, W.G., Yeager, S.G., 2004. Diurnal to decadal global forcing for ocean and sea-ice models: the data sets and flux climatologies. National Center for Atmospheric Research, Boulder, CO, USA, 111pp.

Marchesiello, P., McWilliams, J.C., Shchepetkin, A.F., 2001. Open boundary conditions for long-term integration of regional oceanic models. Ocean Model. 3, 1–20.

Martin, J.H., Gordon, R.M., Fitzwater, S., Broenkow, W.W., 1989. VERTEX-phytoplankton/iron studies in the Gulf of Alaska. Deep-Sea Res. 36, 649–680.

Mass, C.F., Ovens, D., Westrick, K., Colle, B.A., 2002. Does increasing horizontal resolution produce more skillful forecasts? The results of two years of real-time numerical weather prediction over the Pacific Northwest. Bull. Am. Meteor. Soc. 83, 407–430.

Mellor, G.L., Yamada, T., 1974. A hierarchy of turbulence closure models for planetary boundary layers. J. Atmos. Sci. 31, 1791–1806.

Mellor, G.L., Yamada, T., 1982. Development of a turbulence closure-model for geophysical fluid problems. Rev. Geophys. 20, 851–875.

Napp, J.A., Incze, L.S., Ortner, P.B., Siefert, D.L.W., Britt, L., 1996. The plankton of Shelikof Strait, Alaska: standing stock, production, mesoscale variability and their relevance to larval fish survival. Fish. Oceanogr. 5 (Suppl. 1), 19–38.

NGDC, 1988. Data Announcement 88-MGG-02, Digital relief of the surface of the Earth, National Oceanic and Atmospheric Administration, National Geophysical Data Center, Boulder, CO.

Olson, J., Colle, B.A., Bond, N.A., Winstead, N.S., 2007. A comparison of two coastal barrier jets along the southeast Alaskan coast during the SARJET field experiment. Mon. Weather Rev. 135, 2973–2994.

OCSEAP Staff, 1987. Marine fisheries: resources and environment. In: Hood, D.W., Zimmerman, S.T. (Eds.), The Gulf of Alaska Physical Environment and Biological Resources. US Minerals Management Service, Springfield, VA, USA, pp. 417–458.

Okkonen, S.R., Weingartner, T.J., Danielson, S.L., Musgrave, D.L., Schmidt, G.M., 2003. Satellite and hydrographic observations of eddy-induced shelf–slope exchange in the northwestern Gulf of Alaska. J. Geophys. Res.-Oceans 108, 3033.

Parkinson, C.I., Washington, W.M., 1979. A large-scale numerical model of sea ice. J. Geophys. Res.-Oceans 84, 331–337.

Royer, T.C., 1981. Baroclinic transport in the Gulf of Alaska. Part II. A fresh water driven coastal current. J. Mar. Res. 39, 251–266.

Royer, T.C., 1982. Coastal fresh-water discharge in the Northeast Pacific. J. Geophys. Res.-Ocean Atmos. 87, 2017–2021.

Royer, T.C., 1998. Coastal processes in the northern North Pacific. In: Robinson, A.R., Brink, K.H. (Eds.), The Sea. Wiley, New York, pp. 395–414.

Sambrotto, R.N., Lorenzen, C.J., 1987. Phytoplankton and primary production. In: Hood, D.W., Zimmerman, S.T. (Eds.), The Gulf of Alaska: Physical Environment and Biological Resources. US Department of Commerce, USA, pp. 249–282.

Shchepetkin, A.F., McWilliams, J.C., 1998. Quasi-monotone advection schemes based on explicit locally adaptive dissipation. Mon. Weather Rev. 126, 1541–1580.

Shchepetkin, A.F., McWilliams, J.C., 2003. A method for computing horizontal pressure-gradient force in an oceanic model with a nonaligned vertical coordinate. J. Geophys. Res.-Oceans 108, 3090.

Simpson, J.H., 1981. The shelf-sea fronts: implications of their existence and behavior. Philos. Trans. Roy. Soc. A 302, 531–546.

Stabeno, P.J., Bond, N.A., Hermann, A.J., Kachel, N.B., Mordy, C.W., Overland, J.E., 2004. Meteorology and oceanography of the Northern Gulf of Alaska. Cont. Shelf Res. 24, 859–897.

Stabeno, P.J., Hermann, A.J., 1996. An eddy-resolving model of circulation on the western Gulf of Alaska shelf. 2. Comparison of results to oceanographic observations. J. Geophys. Res.-Oceans 101, 1151–1161.

Stabeno, P.J., Reed, R.K., Schumacher, J.D., 1995. The Alaska coastal current: continuity of transport and forcing. J. Geophys. Res.-Oceans 100, 2477–2485.

Stabeno, P.J., Kachel, N., Mordy, C.W., Righi, D., Salo, S.A., 2008. An examination of the physical variability around the Pribilof Islands in 2004. Deep-Sea Res. Pt. II 55, 1701–1716.

US GLOBEC, 1996. US GLOBEC Northeast Pacific implementation plan. US GLOBEC Report no. 17, University of California, Berkeley, CA, 60pp.

Vaz, R.A.N., Simpson, J.H., 1994. Turbulence closure modeling of estuarine stratification. J. Geophys. Res.-Oceans 99, 16143–16160.

Weingartner, T.J., Coyle, K.O., Finney, B., Hopcroft, R., Whitledge, T.E., Brodeur, R., Dagg, M., Farley, E., Haidvogel, D.B., Haldorson, L., Hermann, A.J., Hinckley, S., Napp, J., Stabeno, P.J., Kline, T., Lee, C., Lessard, E., Royer, T.C., Strom, S., 2002. The Northeast Pacific GLOBEC Program: coastal Gulf of Alaska. Oceanography 15, 48–63.

Weingartner, T.J., Danielson, S.L., Royer, T.C., 2005. Freshwater variability and predictability in the Alaska coastal current. Deep-Sea Res. Pt. II 52, 169–191.

Williams, W.J., 2003. Idealized modeling of seasonal variation in the Alaska coastal current. Ph.D. Thesis, University of Alaska, Fairbanks, 100pp.

Williams, W.J., Weingartner, T.J., Hermann, A.J., 2007. Idealized three-dimensional modeling of seasonal variation in the Alaska coastal current. J. Geophys. Res. 112, C07001.

Winstead, N.S., Colle, B., Bond, N., Young, G., Olson, J., Loescher, K., Monaldo, F., Thompson, D., Pichel, W., 2006. Barrier jets in the Gulf of Alaska: combining SAR remote sensing, field observations and models to better understand coastal flows in the Gulf of Alaska. Bull. Am. Meteorol. Soc. 87, 787–800.

Zagar, N., Zagar, M., Cedilnik, J., Gregoric, G., Rakovec, J., 2006. Validation of mesoscale low-level winds obtained by dynamical downscaling of ERA40 over complex terrain. Tellus 58A, 445–455.

Zillman, J.W., 1972. A study of some aspects of the radiation and heat budgets of the southern hemisphere oceans. Department of the Interior, Canberra, Australia, 562pp.